Department of Pathobiology
University of Veterinary Medicine Vienna

Institute of Pathology
(Head: Prof. Dr. Herbert Weissenböck)

Effects of exogenous lipid stimulation on tumor invasiveness in canine osteosarcoma *in vitro*

Diplomarbeit

University of Veterinary Medicine Vienna

submitted by
Nicolle Gobbo Oliveira Erünlü

Vienna, July 2020

Betreuerin: Mag.rer.nat. Cordula Gabriel, PhD

Contents

1 Introduction

1.1 Osteosarcoma and the lipid metabolism

Bone cancer affects humans and animals, in fact osteosarcoma is the most common primary malignancy of bone. Osteosarcoma affects most often metaphyseal areas of rapidly growing long bones, having a dysfunctional activity of osteoblast, osteoclast and mesenchymal precursors. Osteosarcoma is an aggressive tumor, frequently affecting lung and other bones in metastatic disease (De Luca, et al., 2018).

Osteosarcomas occurs more often in appendicular skeleton rather than in axial skeleton, both in humans and dogs. Different factors can influence the incidence rate, for dogs it can be the body weight, breed, neutering status, sex, and others. Diagnostic and prognostic tools are extremely important for osteosarcoma treatment, as surgery and chemotherapy have currently the best treatment outcome (Simpson, et al., 2017).

Early detection and control of metastasis is the biggest challenge. Researches are investigating new ways to approach the cancer and its treatment, the lipids have been showing they are important signaling molecules, maintaining structural integrity, storing energy, in addition to that they can also be reprogrammed in cancerous states. The understanding of the pathways and mechanisms connecting cancer and lipid metabolism can provide new options for treatments and maybe different prognosis (Roy, Dibaeinia, Fan, Sinha, & Das, 2019).

Alterations in lipid metabolism are related to immune disorders and cancer. The cancer cells metabolism changes and adapts to support continuous growth and proliferation, providing lipids, nucleic acids, and proteins necessaries for the oncogenic processes (Roy, Dibaeinia, Fan, Sinha, & Das, 2019).

Studies have found that hypercholesterolemia and a high-fat high-cholesterol diet can affect cancer development (Ding, Zhang, Li, & Yang, 2019). Cholesterol (CH) is stored in lipid droplets and the concentration of CH in the cell is controlled by its influx and efflux from the droplet. The expression of genes related to the CH regulation can be modified, resulting in increase in gene copies, CH synthesis gene expression and CH import by low density lipid (LDL) receptors, and decreased transport of CH (Roy, Dibaeinia, Fan, Sinha, & Das, 2019).

Another lipid of interest is the OA, it has been demonstrated the inhibition in cell proliferation caused by OA in different tumor cell lines. Furthermore, it has been shown that effects of OA support suppressing the invasive progression and metastasis in human cancers. Other possible effects include interfering with the signaling pathways linked to proliferation and being part of apoptotic events (Carrillo, Cavia, & Alonso-Torre, 2012). The demonstrated effects of OA evidence the promising application in cancer therapy, being an alternative or a complement for the traditional protocols. Such effects we would like to test in an *in vitro* environment to confirm the assumptions.

Based on that, our tests target alterations on the cell behavior caused by exogenous CH and oleic acid (OA) provided in an *in vitro* environment.

1.2 Perilipins in lipids and cancer metabolism

Lipid droplets are involved in cellular lipid accumulation, storage, metabolism and cellular physiology. Perilipins (PLINs) are proteins coating the surface of lipid droplets, changing according to different physiological conditions. These proteins serve as controllers and messengers, interacting with cytosolic proteins and organelles controlling cellular lipid homeostasis, composed by five members of the PLIN family (Khor, Shen, & Kraemer, 2013).

PLIN1 is mainly expressed in white adipocytes and participates in the regulation of lipolysis through changes of its phosphorylation status and its interaction with lipases and lipase activators. PLIN1 also promotes the enlargement of lipid droplets (Khor, Shen, & Kraemer, 2013).

PLIN2 is extensively expressed and interacts with lipid droplets surface lipids like phosphatidylcholine, CH, sphingomyelin and stearic acid. Overexpression of PLIN2 increases cellular phospholipid content, indicating its participations in expanding lipid droplet membrane size to adapted droplet expansion during lipid accumulation. Silencing PLIN2 has being proved to reduce the growth of tumor cells (Khor, Shen, & Kraemer, 2013).

PLIN3 is mainly present in hepatocytes, enterocytes, and macrophages, and the expression increases in consequence to lipid loading. PLIN3 can be found in the cytoplasm and it is involved in recycling processes and lipid biogenesis (Khor, Shen, & Kraemer, 2013).

PLIN4 is located in the cytosol, being expressed in adipocytes and, like PLIN1, PLIN4 appears in the last stages of the adipocyte differentiation. Under the adipogenic influence, PLIN4 coats nascent LDs simultaneously with PLIN3 and PLIN2 (Khor, Shen, & Kraemer, 2013).

Expressed in oxidative tissues, PLIN5, localizes in lipid droplets, mitochondria and in nuclear fractions. PLIN5 increases lipid accumulation, to enhance fatty acid oxidation, to sequester fatty acid from excessive oxidation. Cytosolic pools of PLIN5 are connected to structures of high-density lipid droplets and could be intracellular sites for lipid accumulation, and potential shifts to larger lipid droplets upon lipid loading (Khor, Shen, & Kraemer, 2013). During catecholamine-stimulated lipolysis PLIN5 enriches in the nucleus, acting as transcriptional co-regulator that helps to match mitochondrial capacity to the lipid load (Gallardo-Montejano, et al., 2016).

The tumor progression is defined by constant proliferative signaling, invasion and metastasis, prolonging cell immortality (Shyu Jr, Wong, Crasta, & Thibault, 2018). Lipids in cancer are necessary to sustain rapid proliferation rate and high energy consumption, being also responsible for the signaling pathways involved in cell survival, angiogenesis, and metastasis having a second messenger function (Tirinato, et al., 2017).

Lipid upregulation in cancers leads to an upregulation of cell surface receptors for plasma lipids. The upregulation of lipid droplet coating proteins, such as PLINs, exhibited in multiple cancer cells have been shown to promote formation and accumulation of lipid droplets (Diao & Lin, 2019). Evidence suggests that higher levels of lipid droplets are associated with higher tumor aggressiveness, progression and metastasis (Tirinato, et al., 2017) (Roy, Dibaeinia, Fan, Sinha, & Das, 2019), making the lipid droplets a promising target for cancer therapy (Shyu Jr, Wong, Crasta, & Thibault, 2018).

Based on the presented data the current study aimed to investigate the effects of exogenous lipid stimulation on canine osteosarcoma cell behavior *in vitro*. Different cell culture techniques and analytical approaches were applied and will therefore be introduced in the following chapters.

1.3 Two-dimensional and three-dimensional cell culture and invasion assay model

The replication and capacity to predict the human response to drugs represents a challenge, for that we can use available artificial *in vitro* models to represent the *in vivo* conditions.

Osteosarcoma pathogenesis and progression can be investigated using different types of cell culture models (De Luca, et al., 2018). Cell migration is fundamental for biological processes, which is also presented in pathological processes like cancer metastasis. The cancer disseminates throughout the body when the cancer cells migrate and invade through extracellular matrix, intravasate into blood circulation and attach to a distant site (Justus, Leffler, Ruiz-Echevarria, & Yang, 2014).

The transwell migration/invasion assay provides the necessary data to understand how a cell type can spontaneously respond to a chemoattractant and directionally migrate toward it *in vitro*. The cell invasion assay can be performed by adding a layer of extracellular matrix to the transwell membrane to represent the process of extracellular matrix invasion. The transwell invasion assay makes it possible to analyze the cells respond to various chemo attractants and migrate through a physical barrier toward it (Justus, Leffler, Ruiz-Echevarria, & Yang, 2014).

The interaction between cell-cell and cell-matrix also has an important role in tumor morphogenesis and cancer progression, and unfortunately two-dimensional (2D) cell culture models cannot represent real tumor macrostructure and do not represent the multifactorial variations of the tumor microenvironment. The 2D model is also not able to demonstrate physiological cell surface receptors expression, growth factor synthesis and physical and chemical conditions (De Luca, et al., 2018).

Gebhard, et al., 2018 demonstrated that osteosarcoma cell lines can be analyzed with two different methods; the 2D cell monolayer and the three-dimensional (3D) cell culture. In that study using the canine osteosarcoma cell line D17, it was presented that the 3D cell represents better the environment mimicking micro-tumors and metastases *in vitro* in comparison to the corresponding 2D cell culture. Wolfe, et al., 2011 observed that the osteosarcoma cell line OSCA40 presented a spontaneous capacity for metastasis, not present in the cell line D17, making OSCA40 a better model for our invasion assay and the chosen osteosarcoma cell line for our study, reaffirming the importance of the 3D model.

Three-dimensional (3D) invasion assays can be used for a more complete and physiologically representative cancer invasion models. The 3D models like microtumor spheroids *in vitro* are more realistic representations of tumors *in vivo*, and they reproduce similar morphology, cell-cell relations, decreased proliferation rates, increased cell survival, tumor dormancy, and a

hypoxic core. A 3D model thereby provides a more physiological representation for tumor invasion analyses and can be quantitated through image analysis (Trevigen, Inc, 2016).

The application of 3D cell culture systems with scaffold makes possible to control chemical composition, shape, structure, porosity and stiffness of the 3D matrix, influencing cell-cell interaction and proliferative and migratory capabilities of tumor cells (De Luca, et al., 2018).

Tumor cells during a malignant progression invade the surrounding tissue, spreading into distant organs. Cancer cell invadopodia infiltrate the basement membrane and thereby allow the tumor cells to move and to degrade the extracellular matrix. Invadopodia infiltrate the extracellular matrix and are valid structures indicating the importance for tumor cell invasion and metastasis (Vinci, Box, & Eccles, 2015). Studying the invasive capacity of osteosarcomas *in vitro*, invading cells are important factors to consider and therefore, measurement of invadopodia resulting from 3D microtumor models *in vitro* was an additional technique in the present study to determine the effects of exogenous lipid stimulation on invasive behavior of the canine osteosarcoma cells *in vitro.*

1.4 qRT-PCR

The qRT-PCR is used to determine gene expression in different fields. Primers are design to identify specific targets, allowing quantification of functional gene markers present in the analyzed sample. Real time qRT-PCR is a reliable method, reproducible and sensitive enough to quantitatively track functional gene alterations under experimental conditions. The quantitative data produced can be used to relate variations in gene expression with alterations in environment and metabolism (Smith & Osborn, 2009). For the study on hands we identified a set of genes of interest involved in lipid metabolism, cancer invasiveness and metastatic disease.

Adenosine triphosphate binding cassette transporter A1 (ABCA1) works as a phospholipid translocase. Once the phospholipids translocated by ABCA1 are recruited, the newly produced complexes promote CH efflux in an autocrine, paracrine, or even endocrine ways, possibly from specific groups of cellular CH (Wang, Silver, Thiele, & Tall, 2001). ABCA1 correlation with cancer development is due to its capacity to efflux isopentenyl pyrophosphate (IPP), an activator of anti-tumor cells. Also, it has been proposed that the adenosine triphosphate binding

cassette transporter B1 (ABCB1) high/ABCA1 low phenotype is indicative of chemo-immune-resistance in osteosarcomas (Belisario, et al., 2020).

1-acylglycerol-3-phosphate O-acyltransferase (AGPAT9) catalyzes the conversion of glycerol-3-phosphate to lysophosphatidic acid, which converts to phosphatidic acid and subsequently to diglyceride. AGPAT9 is identified as metastasis associated gene 1 and encodes the enzyme Glycerol-3-phosphate acyltransferase 3 (GPAT3) (Roy, Dibaeinia, Fan, Sinha, & Das, 2019).

Glycogen synthase kinase 3 beta (GSK3B) phosphorylates protein substrates and modulates the stability of the targeted protein. GSK-3 is important in cancer development as it participates in signaling pathways, like the nuclear factor kappa B (NF-κB) protein which is commonly deregulated in cancer and can induce pro-inflammatory genes which contribute to cancer progression (Duda, et al., 2020). Shimozaki, et al., 2016 demonstrated that the inhibition of GSK-3β causes the activation of β-catenin, an assumed tumor suppressor in bone and soft tissue sarcoma and an important component of osteogenesis, proving that GSK-3β is important for the survival and proliferation of osteosarcoma cells.

Phospholipid phosphatase 2 (PLPP2) catalyzes the conversion of phosphatase to diglyceride, increasing levels of diglyceride overall. The knock down of PLPP2 can diminish anchorage-dependent *in vitro* growth of cancer cell lines (Roy, Dibaeinia, Fan, Sinha, & Das, 2019). PLPP2 expression has been observed to be elevated in numerous carcinomas and sarcomas (Tang, Benesch, & Brindley, 2015).

Monoglyceride lipase (MGLL) catalyze the hydrolysis of monoglycerides into glycerol and fatty acids, allowing monoglyceride lipase to regulate physiological and pathophysiological processes as monoglycerides and fatty acids function as signaling lipids or precursors (Grabner, Zimmermann, Schicho, & Taschler, 2017). Roy, Dibaeinia, Fan, Sinha, & Das, 2019 observed that AGPAT9, PLPP2, and MGLL were upregulated in diacylglycerol metabolism in metastatic cells in comparison to nonmetastatic cells. Foley, et al., 2015 also observed that MGLL was downregulated in anchorage-independent osteosarcoma cells compared to adherent osteosarcomas cells.

MYC proto-oncogene (MYC), basic helix-loop-helix (bHLH) transcription factor, participates in growth control, differentiation and apoptosis, and its modified expression has been associated with many naturally occurring neoplasms (Hoffman & Liebermann, 1998). C-MYC overexpression also promotes osteosarcoma cell invasion, probably via activation of Mitogen-

activated protein kinase (MEK)- Extracellular signal-regulated kinase (ERK) pathway (Han, Wang, & Bi, 2012).

Oxidized low-density lipoprotein receptor 1 (OLR1) encodes an LDL receptor and regulation is through the cyclic adenosine monophosphate (AMP) signaling pathway. The produced protein binds, internalizes, degrades oxidized LDL, and possibly is related to the regulation of apoptosis antigen 1 -induced apoptosis (U.S. National Library of Medicine, 2020). It has been demonstrated that OLR1 regulates the epithelial to mesenchymal transition (EMT), being involved with the promotion of lung metastases in osteosarcoma (Jiang, et al., 2019).

Sterol regulatory element binding protein 1 (SREBP-1) controls lipid biosynthesis and adipogenesis as it regulates the expression of enzymes necessary for CH, fatty acid, triacylglycerol and phospholipid synthesis. In vertebrates, SREBP activation is controlled by a structure modulated by CH (Bertolio, et al., 2019). SREBP-1 also promotes the gene transcription of enzymes participating in cell migration and invasion in human glioma, osteosarcoma and prostate cancers, modulating the carcinogenic process through molecular signaling pathways (Li, et al., 2014).

Upstream transcription factor 2 (USF2) encodes a component of the bHLH transcription factors involved in the control of cellular proliferation. The produced protein promotes transcription through pyrimidine-rich initiator elements and E-box motifs and participates in the regulation of cellular processes (U.S. National Library of Medicine, 2020). USF2 also plays a tumor-suppression role in prostate carcinogenesis (Chen, et al., 2006). Qyang, et al., 1999 demonstrate that in HeLa cells, the USF proteins overexpression causes noticeable growth inhibition, but has no effect on the proliferation of the Saos-2 osteosarcoma cell line.

Scavenger receptor class B member 2 (SCARB2), also known as lysosomal integral membrane protein type 2 (LIMP-2), is an intracellular transport of CH and it is tightly regulated. SCARB2 reduction alters SREBP-2-mediated CH regulation and LDL-receptor expression. There are indications that SCABR2 transports CH in lysosomes and controls a lysosomal CH export (Heybrock, et al., 2019).

Reference genes are extremely important to guarantee the accuracy of the analyses, they are consistently expressed in the material of study and are essential for the normalization of the target-gene expression. Cancerous tissues have a more variable level of gene expression than normal tissues, making difficult to select a reference gene best representing the internal

reference controls for a range of cancers and being crucial to proof the stability of the reference gene in the analyzed material (Jo, et al., 2019).

Ornithine Decarboxylase Antizyme 1 (OAZ1) encodes a protein belonging to the ornithine decarboxylase antizyme family, which participates in cell growth and proliferation and regulates intracellular polyamine concentration. OAZ1 is considered a universal reference gene and encodes antizyme 1, broadly distributed in the tissue (Medicine, U. N., 2020).

Ribosomal Protein L27 (RPL27) encodes an element of the ribosomal proteins and a component, having multiple processed pseudogenes of this gene distributed through the genome (Medicine, U. N., 2020).

1.5 Immunohistochemistry

Immunohistochemistry (IHC) is an important utilization of monoclonal and polyclonal antibodies to identify the distribution of the antigen of interest on the analyzed tissue. It is commonly used for diagnosis of cancers because specific tumor antigens are upregulated in certain cancers. IHC samples are processed into sections with a microtome and then the sections are incubated with an appropriate antibody. The site of antibody binding is visualized when it is connected to an appropriate secondary antibody (Duraiyan, Govindarajan, Kaliyappan, & Palanisamy, 2012). In IHC approaches antibodies are used to detect protein expression while preserving the composition, cellular characteristics, and structure of the tissue. The precise binding between an antibody and its epitope makes it possible to detect specific sequences, targeting defined regions (Crosby, et al., 2020).

The Ki-67 immunostaining is commonly used as a proliferation marker. The nuclear protein Ki-67 is expressed during the cell cycle but absent in quiescent cells. The Ki-67 staining allows an easy and rapid evaluation of the proliferative state of tumor samples (Marinho, et al., 2005). It has been demonstrated a correlation of Ki67 expression with metastasis, showing that the expression is considerably higher in malignant tissues with poorly differentiated tumor cells in comparison to normal tissue (Li, Jiang, Chen, & Zheng, 2015).

1.6 Western blot

Western blot (WB) is a valuable method to identify specific proteins in a complex mixture of proteins extracted from cells. To perform such analysis, the proteins are separated by size and the target protein is marked using a primary antibody followed by an appropriate secondary detection system (secondary antibody) to make visible the detected proteins on the membrane. The antibodies bind to the protein of interest are visible in a band, which the thickness represents the protein concentration (Mahmood & Yang, 2012). Variations can be observed, for that reason it is important to normalize the obtained values relative to the reference band.

1.7 Hypotheses

In the study on hand it was hypothesized, that exogenous CH but not OA stimulation enhances invasive capacity of the canine osteosarcoma cells. Two different models (2D and 3D invasion assay) were applied to identify the effects of exogenous lipid stimulation on the invasive behavior of the cells. We furthermore assumed, that exogenous lipid stimulation enhances (CH) or reduces (OA) proliferative activity of canine osteosarcoma cells *in vitro*. To investigate this hypothesis a 3D microtumor model of canine OSCA40 osteosarcoma cells was applied and spheroids were analyzed by means of anti-Ki67 immunohistochemical staining. The same samples were used for detection of PLINs expression by means of qRT-PCR, WB and IHC as it was assumed that exogenous lipid stimulation induces changes of PLINs expression on mRNA and protein levels. Additionally, we hypothesized that pro-oncogenic and metastatic disease related genes we up (CH) or down (OA) regulated by exogenous lipid stimulation in the 3D canine osteosarcoma microtumor models *in vitro*. Therefore, we applied real time qRT-PCR searching for regulative effects on different genes of interest in the stimulated canine osteosarcoma models *in vitro*.

2 Material and Methods

2.1 Preparing the medium

In all experimental set ups medium Dulbecco's Modified Eagle Medium (DMEM) high glucose, containing fetal calf serum (FCS) (10 %), antibiotic/antimycotic solution 100x (1 %), and L-glutamine (1 %) was used as standard medium.

2.2 Preparing cells for two-dimensional invasion assay

The canine osteosarcoma cell line OSCA40 cells were placed in a tissue culture flask 75 (T75) at 30 % confluence in culture medium and separated in four different treatments; CH, OA, CH + OA and standard medium for the control group (C); in a concentration 4 µl/ml, 0,1 µl/ml, 4 µl/ml + 0,1 µl/ml and no treatment, respectively and incubated for 2 days (at 37 ◦C and 5 % CO_2). The cells were rinsed three times with 6 ml of 1x Phosphate-Buffered Saline (PBS) and the 1x PBS removed carefully, then added 2 ml of trypsin and placed in the incubator for 2 minutes. The trypsin digestion was stopped by adding 4 ml medium. The cell suspension was centrifuged at 500 g for 2 minutes. The medium was removed and the pellet was resuspended in 1 ml fresh medium. A hemocytometer was used to determinate the cell concentration, the suspension was diluted to a cell density of $1{,}5.10^4$ cells/ml. 24 transwells (Transwell®, VWR, Austria) featuring 8 µm pore diameter were incubated with 25 µl coating fluid (Geltrex® Gibco™) per insert for 60 minutes for gelling (at 37 ◦C and 5 % CO_2). The bottom side of the transwell was washed twice with serum free medium**.** In this experiment we incubated six transwells per treatment. Into each well of a 24 well plate was added 500 µl of culture medium containing 10 % FCS and the treatments CH, OA, CH + OA or C, in a concentration 4 µl/ml, 0,1 µl/ml, 4 µl/ml + 0,1 µl/ml and no treatment, respectively. The transwells were transferred into each well of the 24 well plate. 400 µl of cell suspension at final cell density of $1{,}5.10^4$ cells/ml was added to each transwells ´upper chamber and incubated for 24 hours (at 37 ◦C and 5 % CO_2). The cells were fixed in 4 % formol for 15 minutes at room temperature. The medium and the formol were removed and the transwell was washed twice in both sides of the membrane with double distilled water. The cells were stained using hematoxylin, adding 500 µl per well and incubating for 5 minutes at room temperature. The transwell was washed twice with tap

water and incubated for 10 minutes at room temperature. The upper chamber from each transwell was cleaned with a cotton swab. Images were captured using a live cell imaging station (Evos7000, Thermo Fisher Scientific, Austria) from different fields in order to cover up all the surface of the transwell using 10x and 4x objectives.

2.3 Preparing cells for spheroids

The OSCA40 cells were placed in a T75 flask at 30 % confluence and incubated for 2 days (at 37 ◦C and 5 % CO_2) in standard culture medium. The cells were rinsed three times with 6 ml of 1x PBS and the 1x PBS removed carefully, then added 2 ml of trypsin and placed in the incubator for 2 minutes. The trypsin digestion was stopped by adding 4 ml medium. The cell suspension was centrifuged at 500 g for 2 minutes. The medium was removed and the pellet was resuspended in 1 ml fresh medium. A hemocytometer was used to determinate the cell concentration, and the suspension was diluted to a cell density of 2.10^3 cells/ml. The suspension was transferred to 96 well plates with rounded wells (Corning® Brand 96-Well, VWR, Austria) using a multichannel pipette, pipetting 100 µl per well, and incubated for 3 days (at 37 ◦C and 5 % CO_2). The OSCA40 spheroids were stimulated with four separated treatments, per well 100 µl medium was added containing the treatments CH, OA, CH + OA or C to the 96 well plates, in a final concentration 4 µl/ml, 0,1 µl/ml, 4 µl/ml + 0,1 µl/ml and no treatment per well (C), respectively, and incubated for 2 days (at 37 ◦C and 5 % CO_2). The medium was removed from each well and it was added 100 µl fresh medium containing the treatments CH, OA, CH + OA or C to the 96 well plates, in a final concentration 4 µl/ml, 0,1 µl/ml, 4 µl/ml + 0,1 µl/ml and no treatment per well, respectively, and incubated for 2 days (at 37 ◦C and 5 % CO_2). One more time the medium was removed from each well and per well was added 100 µl fresh medium containing the treatments CH, OA, CH + OA or C to the 96 well plates, in a final concentration 4 µl/ml, 0,1 µl/ml, 4 µl/ml + 0,1 µl/ml and no treatment per well, respectively, and incubated for 2 days (at 37 ◦C and 5 % CO_2). The spheroids were used for the 3D invasion assay, qRT-PCR, WB and IHC.

2.4 Preparing three-dimensional invasion assay

For the 3D invasion assay 24 spheroids were collected as described above, stimulating six spheroids for each of the four different treatments. A 24 well Matrigel plate (Corning™ BioCoat™ Matrigel Matrix Multiwellplatten, VWR, Austria) was thawed in the fridge overnight. 200 µl medium containing the treatments CH, OA, CH + OA or C was added to each well, in a final concentration 4 µl/ml, 0,1 µl/ml, 4 µl/ml + 0,1 µl/ml and no treatment per well, respectively, and incubate for 30 minutes (at 37 ◦C and 5 % CO_2). The spheroids were transferred individually from the 96 well plate and placed on the transition between the medium and the Matrigel and incubated (at 37 ◦C and 5 % CO_2). Photos were taken of each well at 0, 24, 48, 72, 96, 120, 144 and 168 hours with microscope (Zeiss Axio Observer Z1 Inverted, Carl Zeiss Microscopy, Germany) using 4x and 10x objectives. Images were analyzed with the free software FIJI by ImageJ, measuring the spheroids ´area and the length of the invadopodia.

2.5 Preparing spheroids for qRT-PCR

Spheroids (32) of each group were collected, pooled and transferred from the 96 well plate to a 15 ml tube, centrifuged for 2 minutes at 500 g and the medium was removed. 2 ml 1x PBS was added, centrifuged for 2 minutes at 500 g and the 1x PBS was removed. 350 µl QIAzol® was added to the tube, the suspension was transferred to a 1 ml collection tube and incubated for 15 minutes at room temperature. The suspension was homogenized using a vortexer. The material was placed in liquid nitrogen and stored at -80 °C.

2.6 Preparing qRT-PCR

The sample preparation was made using Direct-zol™ RNA MiniPrep (Zymo Research Corp.). The samples were thawed and transferred to a collection tube containing bead beaters and homogenized in a high-speed homogenizer at room temperature and centrifugation at 10,000 g for 30 seconds. 350 µl of ethanol was added to the lysed sample. The suspension was transferred to a Zymo-Spin™ IICR Column2 in a collection Tube and centrifuged at 10,000 g for 30 seconds. The column was transferred into a new collection tube and discarded the liquid. 400 µl RNA Wash Buffer was added to the column and centrifuged at 10,000 g for 30 seconds. In a new collection tube 5 µl DNase I was mixed to 75 µl DNA Digestion Buffer, added to the

column matrix and incubated at room temperature for 15 minutes. 400 µl Direct-zol™ RNA PreWash5 was added to the column and centrifuged at 10,000 g for 30 seconds, the flow-through was discarded and repeated this step. 700 µl RNA Wash Buffer was added to the column and centrifuged for 2 minutes at 10,000 g. The column was transferred into a new tube. 50 µl of DNase/RNase-Free Water was added directly to the column matrix and centrifuge. The sample was stored at -80 °C. The complementary DNA (cDNA) preparation was made using High Capacity cDNA Reverse Transcription Kits® (Applied Biosystems, 2016). Thawed the 2x reverse transcriptase (RT) master mix on ice. Placed on ice the collection tube, added the 10x RT Buffer, 25x dNTP Mix, 10x RT Random Primers, MultiScribe™ Reverse Transcriptase, RNase Inhibitor, the same was prepared without the RNase Inhibitor and mixed gently. Next, 10 µl of 2x RT master mix was pipetted into each well of a 96 well reaction plate. 10 µl of RNA sample was pipetted into each well, then mixed. The plates were sealed and centrifuge to bring down the components and to eliminate bubbles. The plates were placed in the thermal cycler and ran the reverse transcription. The cDNA was stored at -15 °C. The samples were thawed and vortexed before the qRT-PCR. In a collection tube it was added distilled water, 5x High-Fidelity mastermix (HF MM), Primer F-R and Primer R. A plate was prepared for each marker, pipetting 18µl of the prepared mixture containing the specific Primers for the test. 2 µl of the prepared cDNA was added to each well. The samples ran in three stages, stage one at 95 ℃ for 12 min, stage two at 95 ℃ for 15 seconds and at 60 ℃ for 1 minute (40 times), stage three at 95 ℃ for 15 seconds, at 60 ℃ for 1 minute and 95 ℃ for 15 seconds, the table 1 shows the primer sequence for each gene tested. The results were analyzed using the Agilent AriaMx™ program. Fold change was used to analyze the genes expression of treated groups and C. The efficiency of the qRT-PCR was calculated for each gene and measured the fold change using the follow formula:

Delta cycle threshold (ΔCt) = cycle threshold (Ct)(target) − Ct(reference)

$\Delta\Delta Ct = \Delta Ct(\text{treated}) - \Delta Ct(C)$

Fold Change = $2^{-\Delta\Delta Ct}$

Tab. 1: Target genes of relevance in cancer cells and metastatic disease, primers sequences and product length applied in the present study to be detected in prepared OSCA40 cell line spheroids using qRT-PCR method.

Target	Forward	Reverse	Amplicon size (bp)
ABCA1	GGTACGAGGACAACAACTACAA	TGCGGGAAAGAGGACTAGA	138
GPAT3	CCTCTCTGGCACCATTCAT	ACCATAGCATAGCATCCATCC	126
GSK3B	CCACAGAACCTCTTGTTGGAT	TACGAAACATTGGGTTCTCCTC	98
MGLL	GGCTTCCTGTCTTCCTTCTG	GGCAAGAACCAAAGGTGAAATC	116
MYC	GCTGCACGAGGAGACAC	CCACAGAAACAACATCAATTTCTTC	86
OLR1	GGGATCCTTTGCTTGGGATTA	GGTGAGTAAGGTTTGCTTGTTG	103
PLPP2	GTGTCAACTGCTCGCTGTA	AAGGAGGAGTGTCCGGAATA	103
SREBF1	CCATCTGTGAGAAGGCTAGTG	GGAGCAAGTCACACAGGAG	105
USF2	GAACACCACGGGATGAAAGA	TCTGCGTTACAATCTGGAATGA	118
PLIN5	CACTTCCTGCCCATGACTG	CACAAAGTAGCCCTGATGTCTC	108
PLIN1	GTACCCTCCTGAGAAGATTG	GGGCACACTGATGCTATT	85
PLIN2	AATTTGCCAGAAAGAATGTGCAT	TCCACCCAGGAGAGGTAGAACTT	79
PLIN3	GGGTCAGGAGAAACTACAC	GTCTCCACCTCTGGTTTG	93
PLIN4	CACCTTCGGACAAGATGA	CCTTTAGCTGTGTCTACCAT	112
SCARB2	CCTACATTGTCATGGCGCTG	GCCTCCGTTAGGTTAGGTTCGTA	140
OAZ1	CTGCTGTAGTAACCTGGGTC	ACATTCAGCCGATTATCAGAGTA	145
RPL27	ACTACAATCACCTCATGCCC	CTTGTACCTCTCCTCGAACTTG	143

2.7 Preparing spheroids for immunohistochemistry

The spheroids were transferred from the 96 well plate to a 15 ml tube, centrifuged for 2 minutes at 500 g and the medium was removed. 2 ml 1x PBS was added, centrifuged for 2 minutes at 500 g and the 1x PBS was removed. 2 ml formol 4 % was added and incubated for 24 hours at room temperature. The formol was removed and added 2 ml ethanol 70 % to the samples and incubated at temperature room for 48 hours. Ethanol was removed from the tube, 500 µl Histogel (Richard-Allan Scientific™ HistoGel™, Thermo Scientific Vienna, Austria) was added to the sample and incubated at 5 °C for 15 minutes. The solidified gel was removed from the tube, cut in the middle and placed in an embedding cassette, immersed in ethanol 70 % until the embedding at the same day. For immunohistochemistry analysis 96 spheroids were pooled and collected as described above.

2.8 Preparing immunohistochemistry

The samples preparation/fixation was performed using automated embedding station (Tissue-Tek® VIP, Sakura, USA). Samples were prepared in paraffin blocks and cooled for the serial section. Formalin fixed and paraffin embedded (FFPE) samples: Serial sections (3µm thickness) were cut from the FFPE samples using a microtome (HM355S, Thermo Scientific, Germany) and mounted on 3-aminopropyltriethoxysilane/glutaraldehyde - coated slides. Following 18 hours drying step, sections were either stained with Hematoxylin and Eosin (H&E) according to Mulisch & Welsch, 2010 for morphological analyses or prepared for the following IHC analyses. For IHC, the slides were incubated for 8 minutes in xylene, repeating once this step. The slides were incubated for 3 minutes in ethanol 100 %, repeating once this step. The slides were incubated for 3 minutes in ethanol 96 %. The slides were incubated for 3 minutes in ethanol 70 %. The endogenous peroxidase was blocked using 40 ml methanol + 1 ml 30 % hydrogen peroxide (H_2O_2) + 9 ml water for 15 minutes. The slides were washed ten times in tap water. Antigen retrieval (steamer) was made using Citratebuffer 0,01 M pH 6,0 for 30 minutes. Slides were cool down for 30 minutes. The slides were washed two times for 5 minutes in 1x PBS. The unspecific binding sites were blocked applying 1,5 % Normal Goat Serum in PBS for 30 minutes (150 µl Normal Goat Serum + 10 ml PBS). 100 µl primary antibody was use per slide, 37x Mouse-anti-Ki67 (MIB1) 1:1000 in PBS prepared 4 µl + 3996 µl PBS for Ki67 detection, see the table 2 for PLIN1, PLIN2, PLIN3, PLIN5; for sources, pre-treatments and dilutions. Slides were incubated overnight at 4 °C. The next day the slides were washed two times for 5 minutes in 1x PBS). 100 µl secondary antibody was use per slide, Bright Vision Poly-HRC-anti-Mouse (Immunologic) for 30 minutes for Ki67 detection, see the table 2 for PLIN1, PLIN2, PLIN3, PLIN5; for sources, pre-treatments and dilutions. Slides were washed twice for 5 minutes in 1x PBS. The slides were incubated with diaminobenzidine (DAB)-solution (Quanto, Richard Allan Scientific, TA-125-QHDX), first preparing 1 ml puffer + 1 drop of DAB chromogen, adding 1-2 drops of the solution per slide and then incubating for 5 minutes. Slides were washed in WEK-Water. The positive control (C+) and negative control (C-) slides were checked using microscope. Nuclei staining was performed for 3 minutes using hematoxylin. Slides were washed for 10 minutes under running tap water. The slides were incubated for 3 minutes in ethanol 96 %. The slides were incubated for 3 minutes in ethanol 100 %, repeating once this step. The slides were incubated for 3 minutes in xylene, repeating

once this step. Slides were mounted with xylene-soluble medium (DPX, Fluka, Buchs, Switzerland). C-s were performed by substitution of the primary antibodies with PBS. Examination of the sections was performed using light microscopy (Polyvar) with a digital DS-Fi1 camera (Nikon, Vienna, Austria) and Nikon NIS elements software. The Ki67 counting was performed using an automated, open source image processing program (FIJI by ImageJ).

Tab. 2: Characterization, sources, treatment and dilutions of the respective antibodies of the PLIN family members PLIN1, PLIN2, PLIN3 and PLIN5 to be detected in canine FFPE tissue samples by means of IHC.

Antibody	Source	Clone	Pretreatment	Dilution	Secondary System	Manufacturer, Cat.
PLIN1	Rabbit	Poly	30min 0,01M Citratebuffer pH6,0	1:10.000	Bright Vision Poly-HRP-anti-rabbit	Abcam, ab3526
PLIN2	Mouse	AP125	30min 0,01M Citratebuffer pH6,0	1:500	Bright Vision Poly-HRP-anti-mouse	AntikörperOnline.de, ABIN112185
PLIN3 (TIP47)	Mouse	F-10	no pretreatment	1:800	Bright Vision Poly HRP-anti-mouse	Santa Cruz, sc- 390968
PLIN5 (LSDP5)	Mouse	E-3	30min 0,01M Citratebuffer pH6,0	1:200	Bright Vision Poly-HRP-anti-mouse	Santa Cruz, sc- 514296

2.9 Preparing spheroids for western blot

The spheroids were transferred from the 96 well plate to a 15 ml tube, centrifuged for 2 minutes at 500 g and the medium was removed. The sample was washed with 1x PBS three times, 2 ml 1x PBS was added, centrifuged for 2 minutes at 500 g and the 1x PBS was removed. 1 ml 1x PBS was added and the suspension was transferred to a collection tube. The tube was centrifuged for 2 minutes at 500 g and the 1x PBS was removed. The dry pellet was placed in liquid nitrogen and stored at -80 °C. For WB analysis 64 spheroids were pooled and collected as described above.

2.10 Preparing western blot

For lysate preparation, the radioimmunoprecipitation assay (RIPA) lysis puffer was added to the pellet and the sample suspension was thawed on ice in (table 3). RIPA lysis buffer contained 50mM Tris hydrochloride (Tris-HCl) pH 7,4, 500 mM sodium chloride (NaCl), 1 % Nonidet

P-40, 0,5 % Na-deoxycholate and 0,1 % sodium dodecyl sulfate (SDS). Before using, it was added 10 µl of proteinase inhibitor cocktail (Sigma Aldrich) and 10 µl phosphatase inhibitor cocktail (Sigma Aldrich) per ml lysis buffer. For mechanical support of the digestion, a hypodermic needle (size 23Gx1 ¼") was used repeatedly (Braun, Germany). The samples' protein concentration was measured using a plate reader (Tecan Infinite 200 PRO, TECAN, Austria).

Protein lysates were separated on 10 % gradient gels by sodium dodecyl sulfate polyacrylamide gel electrophoresis (SDS-PAGE; self-made). Total protein amount for each sample was approximately 20 µg determined with the DC Protein Assay (BioRad, Germany). Proteins were then transferred to polyvinylidene difluoride (PVDF) membranes that were blocked with 5 % (w/v) non-fat dry milk in Tris-Buffered-Saline-Tween (TBST) for PLIN2 and TBST together with WB Blocking Reagent (Roche) in a ratio 1:10 for PLIN1, PLIN3 and PLIN5, respectively. Subsequently, membranes were incubated over night at 4 °C with appropriate dilutions of primary antibody (table 3). On the following day, the membranes were washed in five washing steps using TBST for 8 minutes each, and consecutively incubated with the respective secondary antibody (table 3) at room temperature for 30 minutes. Washing steps were repeated four times with TBST followed by a TBS wash for 8 minutes each. Chemiluminescent signals were detected using the Enhanced Chemiluminescence (ECL) Western Blotting Detection Reagents (Amersham, United Kingdom) and visualized with the BioRad ChemiDoc Imaging System (BioRad). Semiquantitave analysis of the specific bands was performed and the bands presented numerical values that are relative to the reference band for each sample.

Tab. 3: Antibodies' sources, dilutions, lysis buffer and blocking reagent of PLIN1, PLIN2, PLIN3 and PLIN5 to be detected in prepared OSCA40 cell line spheroids using WB.

Primary antibody	PLIN1 (abcam ab3526)	PLIN2 (Proteintech 15294-1-AP)	PLIN3 (SantaCruz, sc-390968)	PLIN5 (ThermoFisher PA1-46215)
Sample	canine adipose tissue	HepG2 human liver cancer cells	canine muscle tissue	canine heart tissue
Lysis buffer	RIPA lysis buffer	RIPA lysis buffer	RIPA lysis buffer	RIPA lysis buffer
Primary antibody dilution	1:500	1:500	1:500	1:4000
Secondary antibody	Donkey Anti-Rabbit IgG Antibody (HRP-linked) (Amersham, NA 934)	Donkey Anti-Rabbit IgG Antibody (HRP-linked) (Amersham, NA 934)	Sheep Anti-Mouse IgG Antibody (HRP-linked) (Amersham, NA 931)	Donkey Anti-Rabbit IgG Antibody (HRP-linked) (Amersham, NA 934)
Blocking Reagent	Western Blocking Reagent (Roche, 11921673001)	5% (w/v) milk powder in TBST	Western Blocking Reagent (Roche, 11921673001)	Western Blocking Reagent (Roche, 11921673001)

2.11 Statistical analysis

All statistical analyses were performed using the GraphPad Prism 8.4.2 with 95 % confidence intervals. Normal distribution of the variables was checked by Kolmogorov-Smirnov method. For the 2D invasion assay, 3D invasion assay and IHC Ki67 counting, the parametric data was analyzed with one-way analysis of variance followed by Tukey's test, the non-parametric data was analyzed with Kruskal-Wallis test followed by Dunn´s test to calculate significance. For the qRT-PCR and the WB, the data was analyzed with Unpaired t-test with Welch's correction to calculate significance. A value $p<0.05$ was considered statistically significant. Three independent experiments were performed for each method of analysis using the same protocol.

3 Results

3.1 Two-dimensional invasion assay

The figure 1 shows the results obtained in relation to the invasion of OSCA40 cells at 24 hours for each experiment. Figures 2 and 3 show the results obtained in relation to the invasion of OSCA40 cells at 24 hours for each treatment. The experiment 1 (exp 1) showed an increase in the invasion of OSCA40 cells stimulated with CH in relation to C at 24 hours analysis ($p<0.05$). The experiment 2 (exp 2) showed an increase in the invasion of OSCA40 cells stimulated with CH+OA in relation to C at 24 hours analysis ($p<0.05$). The experiment 3 (exp 3) showed no effects upon the invasion of OSCA40 cells stimulated with CH, OA and CH+OA in relation to C at 24 hours analysis ($p>0.05$).

Also, when comparing the different experiments with each other, we observed a variation in the invasion of OSCA40 cells in the presence of CH, OA, CH+OA and C ($p <0.05$). The C groups showed variation in the invasion of OSCA40 cells between the experiments. The exp 2 showed an increase in the invasion of OSCA40 cells in relation to the exp 1 of C at 24 hours analysis ($p<0.001$). The exp 3 showed an increase in the invasion of OSCA40 cells in relation to the exp 1 ($p<0.0001$) and exp 2 ($p<0.05$) of C at 24 hours analysis.

The groups stimulated with CH showed variation in the invasion of OSCA40 cells between experiments. The exp 3 showed an increase in the invasion of OSCA40 cells in relation to the exp 1 stimulated with CH at 24 hours analysis ($p<0.01$).

The groups stimulated with OA showed variations in the invasion of OSCA40 cells between experiments. The exp 3 showed an increase in the invasion of OSCA40 cells in relation to the exp 1 ($p<0.01$) and exp 2 ($p<0.01$) stimulated with OA at 24 hours analysis.

The groups stimulated with CH + OA showed variation in the invasion of OSCA40 cells between experiments. The exp 3 showed an increase in the invasion of OSCA40 cells in relation to the exp 1 stimulated with CH + OA at 24 hours analysis ($p<0.0001$). The exp 2 showed an increase in the invasion of OSCA40 cells in relation to the exp 1 stimulated with CH + OA at 24 hours analysis ($p<0.0001$).

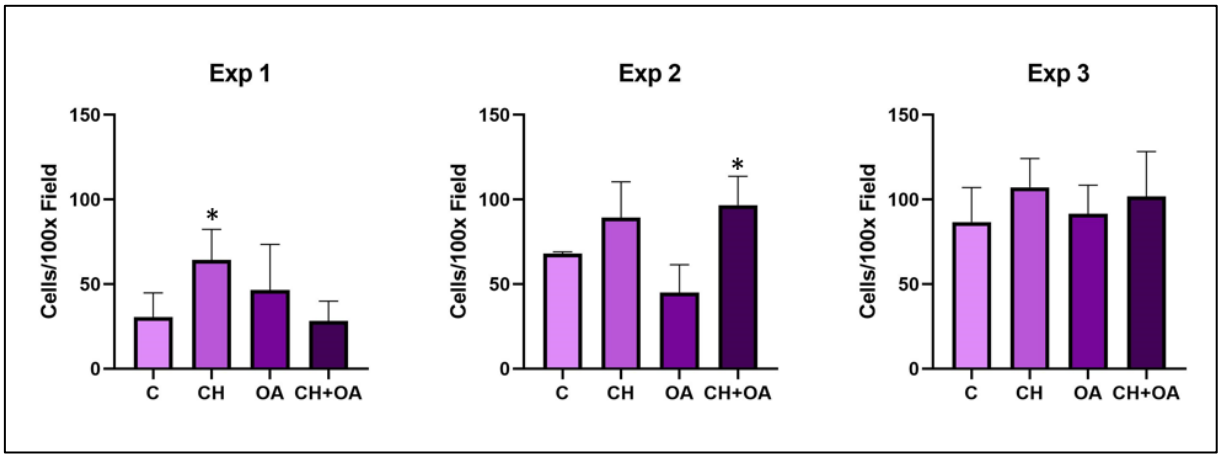

Fig. 1: Effects of CH, OA and CH + OA on the invasion of OSCA40 cells in the 2D invasion assay, stimulated with the respective concentrations of 4 µl/ml, 0,1 µl/ml, 4 µl/ml + 0,1 µl/ml, after a period of 24 hours. The cell counting was performed using 10x magnification in different fields of the transwell, covering the maximum of the insert area. The results represent the mean ± standard deviation of three independent experiments. * $p<0.05$ in relation to C.

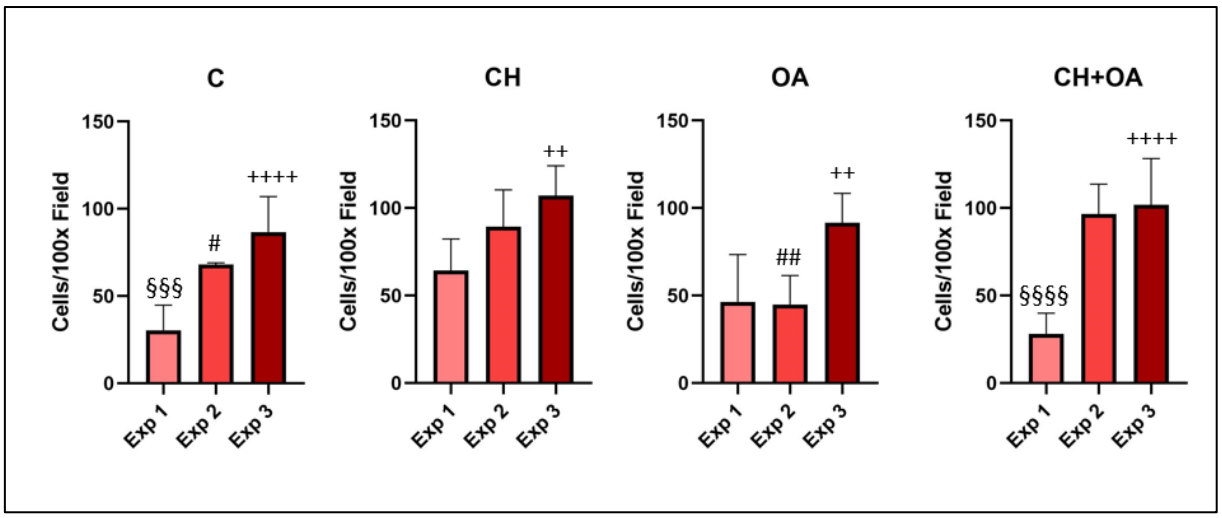

Fig. 2: Variations in the 2D invasion assay between the exp 1, 2 and 3 for each treatment group. The invasion of OSCA40 cells treated with CH, OA and CH + OA and C was analyzed after a 24 hours period. The results represent the mean ± standard deviation. Exp 1 vs. Exp 2 §§§$p<0.001$, §§§§$p<0.0001$; Exp1 vs. Exp 3 ++$p<0.01$, ++++$p<0.0001$; Exp 2 vs. Exp 3 #$p<0.05$, ##$p<0.01$.

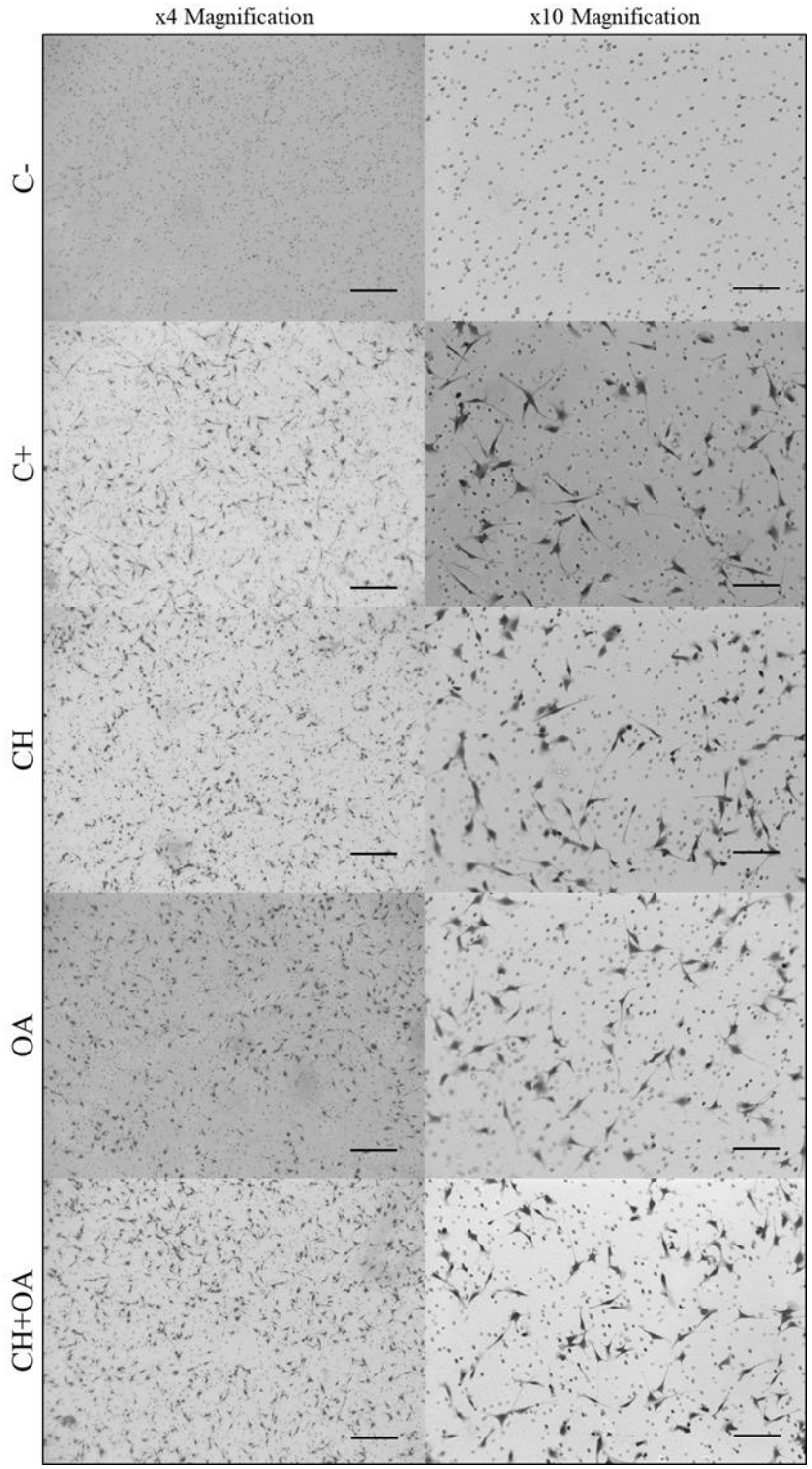

Fig. 3: Representative microphotographs of OSCA40 cells in the 2D invasion assay. Cell invasion was monitored after a period of 24 hours by using hematoxylin staining and documented by using x4 and x10 magnification of a light microscope. The negative C- was without any cells, the C+ was cultured in standard medium and the respective treatment groups contained 4 µl/ml CH, 0,1 µl/ml OA and a combination of 4 µl/ml CH + 0,1 µl/ml OA, respectively (scale x4 magnification = 250 µm; scale x10 magnification = 100 µm).

3.2 Three-dimensional invasion assay

The figures 4 and 5 show the results obtained in relation to the invasion of OSCA40 spheroids for 168 hours for each experiment. Figures 6 and 7 show the results obtained in relation to the invasion of OSCA40 spheroids for 168 hours for each treatment. The exp 1 showed a decrease in the invasion of OSCA40 spheroids stimulated with CH ($p<0.001$), OA ($p<0.001$), CH + OA ($p<0.01$) in relation to the C at 24 hours analysis. The exp 1 showed a decrease in the invasion of OSCA40 spheroids stimulated with CH ($p<0.01$), OA ($p<0.01$), CH + OA ($p<0.01$) in relation to the C at 48 hours analysis. The exp 1 showed a decrease in the invasion of OSCA40 spheroids stimulated with CH in relation to the C at 72 hours analysis ($p<0.05$). The exp 1, exp 2 and exp 3 showed no increase or decrease in the invasion of OSCA40 spheroids stimulated with CH, OA, CH + OA in relation to the C at 96- and 120-hours analyses ($p>0.05$). The exp 3 showed an increase in the invasion of OSCA40 spheroids stimulated with CH in relation to C at 144 hours analysis ($p<0.01$). The exp 2 showed an increase in the invasion of OSCA40 spheroids stimulated with CH + OA in relation to C at 168 hours analysis ($p<0.01$). The exp 3 showed an increase in the invasion of OSCA40 spheroids stimulated with CH ($p<0.0001$), OA ($p>0.05$), CH + OA ($p<0.0001$) in relation to C at 168 hours analysis.

Also, when we analyzed each treatment and compared the different experiments with each other, we observed a variation in the invasion of OSCA40 spheroids in the presence of CH, OA, CH + OA, C ($p <0.05$).

The C groups showed variation in the invasion of OSCA40 spheroids between the experiments. The exp 3 showed an increase in the invasion of OSCA40 spheroids in relation to the exp 2 of C at 24 hours analysis ($p<0.05$). The exp 1, exp 2 and exp 3 showed no increase or decrease in the invasion of OSCA40 spheroids in relation to each other of C at 48- and 72-hours analyses ($p>0.05$). The exp 3 showed an increase in the invasion of OSCA40 spheroids in relation to the exp 2 of C at 96 hours analysis ($p<0.01$). The exp 3 showed an increase in the invasion of OSCA40 spheroids in relation to the exp 2 of C at 120 hours analysis ($p<0.05$). The exp 1 showed an increase in the invasion of OSCA40 spheroids in relation to the exp 2 of C at 144 hours analysis ($p<0.05$). The exp 1, exp 2 and exp 3 showed no increase or decrease in the invasion of OSCA40 spheroids in relation to each other of C at 168 hours analysis ($p>0.05$).

The groups stimulated with CH showed variation in the invasion of OSCA40 spheroids between experiments. The exp 3 showed an increase in the invasion of OSCA40 spheroids in relation to

the exp 1 ($p<0.001$) and to the exp 2 ($p<0.05$) stimulated with CH at 24 hours analysis. The exp 2 showed an increase in the invasion of OSCA40 spheroids in relation to the exp 1 ($p<0.05$) stimulated with CH at 24 hours analysis. The exp 3 showed an increase in the invasion of OSCA40 spheroids in relation to the exp 1 ($p<0.01$) and to the exp 2 ($p<0.05$) stimulated with CH at 48 hours analysis. The exp 3 showed an increase in the invasion of OSCA40 spheroids in relation to the exp 1 stimulated with CH at 72 hours analysis ($p<0.01$). The exp 3 showed an increase in the invasion of OSCA40 spheroids in relation to the exp 1 stimulated with CH at 96 hours analysis ($p<0.01$). The exp 3 showed an increase in the invasion of OSCA40 spheroids in relation to the exp 1 ($p<0.05$) and to the exp 2 ($p<0.05$) stimulated with CH at 120 hours analysis. The exp 3 showed an increase in the invasion of OSCA40 spheroids in relation to the exp 1 ($p<0.05$) and to the exp 2 ($p<0.01$) stimulated with CH at 144 hours analysis. The exp 3 showed an increase in the invasion of OSCA40 spheroids in relation to the exp 1 stimulated with CH at 168 hours analysis ($p<0.05$).

The groups stimulated with OA showed variation in the invasion of OSCA40 spheroids between experiments. The exp 3 showed an increase in the invasion of OSCA40 spheroids in relation to the exp 1 stimulated with OA at 24 hours analysis ($p<0.01$). The exp 1, exp 2 and exp 3 showed no increase or decrease in the invasion of OSCA40 spheroids in relation to each other stimulated with OA at 48-, 72- and 96-hours analyses ($p>0.05$). The exp 3 showed an increase in the invasion of OSCA40 spheroids in relation to the exp 1 stimulated with OA at 120 hours analysis ($p<0.01$). The exp 3 showed an increase in the invasion of OSCA40 spheroids in relation to the exp 1 ($p<0.01$) and to the exp 2 ($p<0.05$) stimulated with OA at 144 hours analysis. The exp 3 showed a decrease in the invasion of OSCA40 spheroids in relation to the exp 2 stimulated with OA at 168 hours analysis ($p<0.05$).

The groups stimulated with CH + OA showed variation in the invasion of OSCA40 spheroids between experiments. The exp 3 showed an increase in the invasion of OSCA40 spheroids in relation to the exp 1 stimulated with CH + OA at 24 hours analysis ($p<0.05$). The exp 1, exp 2 and exp 3 showed no increase or decrease in the invasion of OSCA40 spheroids in relation to each other stimulated with CH + OA at 48- and 72-hours analyses ($p>0.05$). The exp 3 showed an increase in the invasion of OSCA40 spheroids in relation to the exp 1 ($p<0.05$) and to the exp 2 ($p<0.05$) stimulated with CH + OA at 96 hours analysis. The exp 3 showed an increase in the invasion of OSCA40 spheroids in relation to the exp 1 ($p<0.05$) and to the exp 2 ($p<0.05$)

stimulated with CH + OA at 120 hours analysis. The exp 1, exp 2 and exp 3 showed no increase or decrease in the invasion of OSCA40 spheroids in relation to each other stimulated with CH + OA at 144 hours analysis ($p>0.05$). The exp 3 showed an increase in the invasion of OSCA40 spheroids in relation to the exp1 ($p<0.05$) and to the exp 2 ($p<0.01$) stimulated with CH + OA at 168 hours analysis.

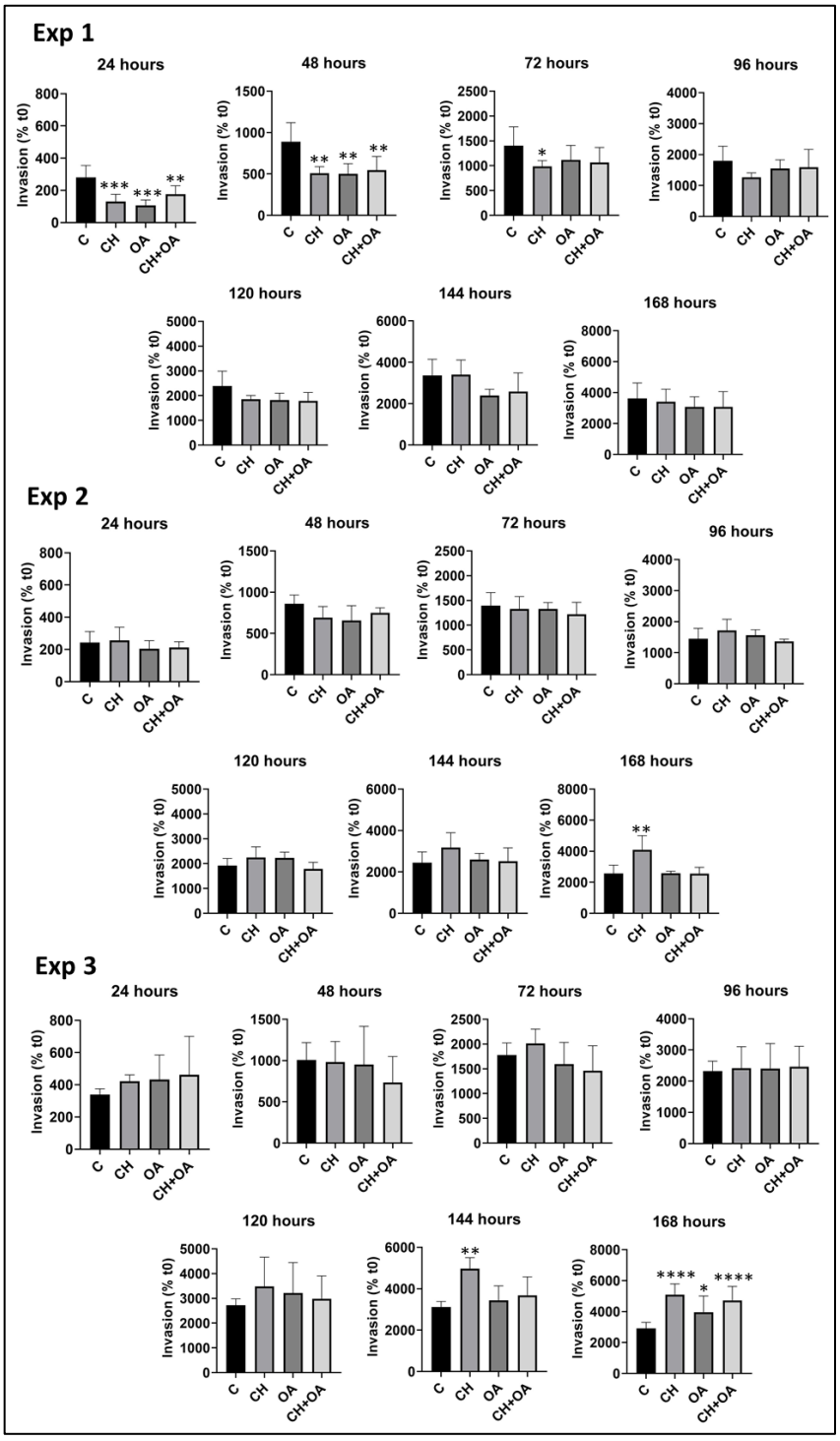

Fig. 4: Graphical representations of three independent experiments (exp 1, exp 2, exp 3) of the 3D invasion assay. OSCA40 spheroids were stimulated with CH, OA, CH + OA with the respective treatment concentrations 4 µl/ml, 0,1 µl/ml, 4 µl/ml + 0,1 µl/ml. The C was incubated with standard medium. The invasion activity (% t0) was calculated considering the growth area at each time point relative to the area in time 0 hour. The invasion activity was observed every 24 hours for a total period of 168 hours. The results represent the mean ± standard deviation. *p<0.05, **p<0.01, ***p<0.001, ****p<0.0001 in relation to C of each time analysis.

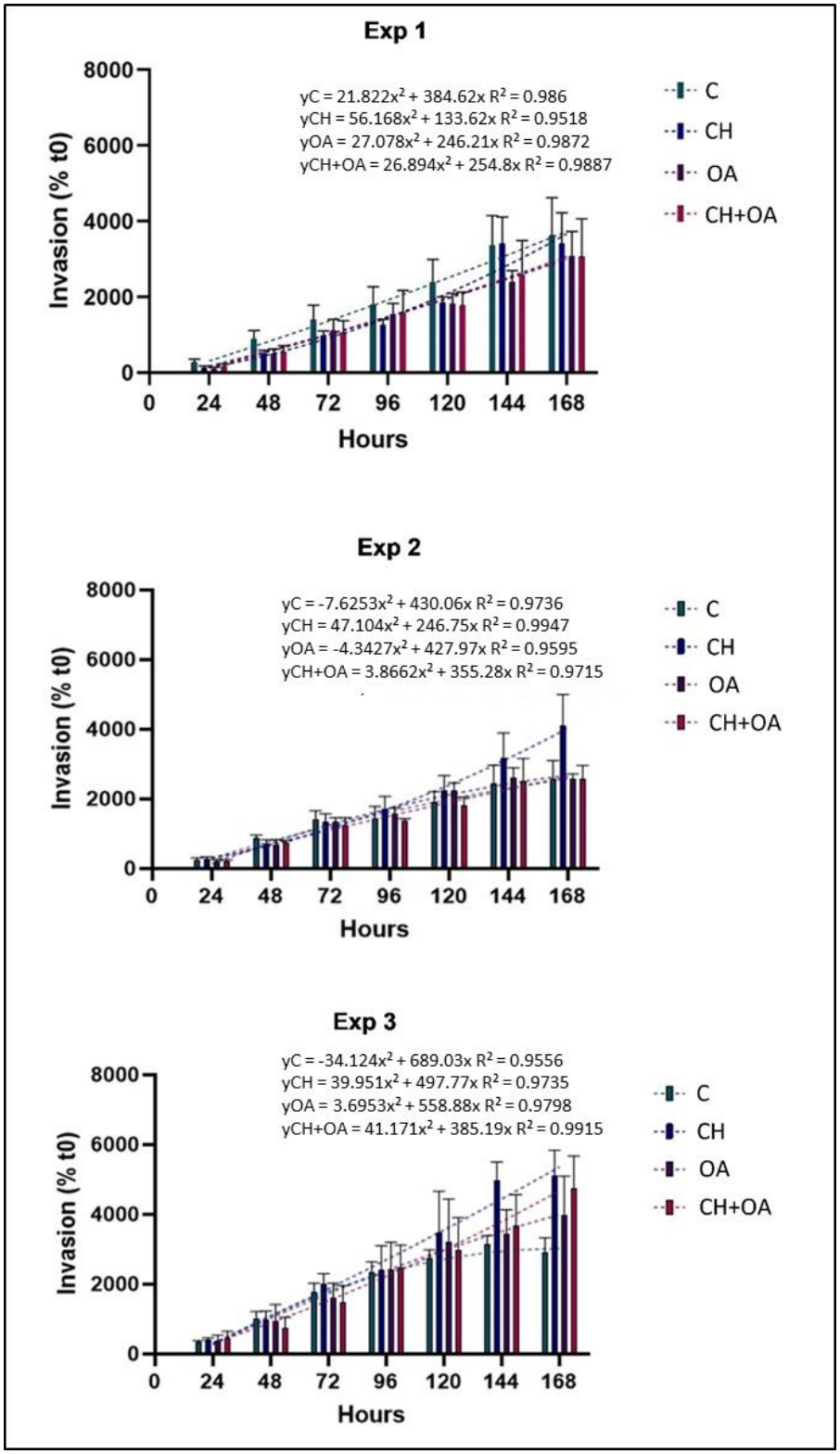

Fig. 5: Observations of the 3D invasion assay in three independent experiments (exp 1, exp 2, exp 3). OSCA40 spheroids were stimulated with CH, OA, CH + OA, and C. The analyses performed every 24 hours are represented with the regression lines, demonstrating the invasion activity of OSCA40 spheroids throughout the 168 hours of observation.

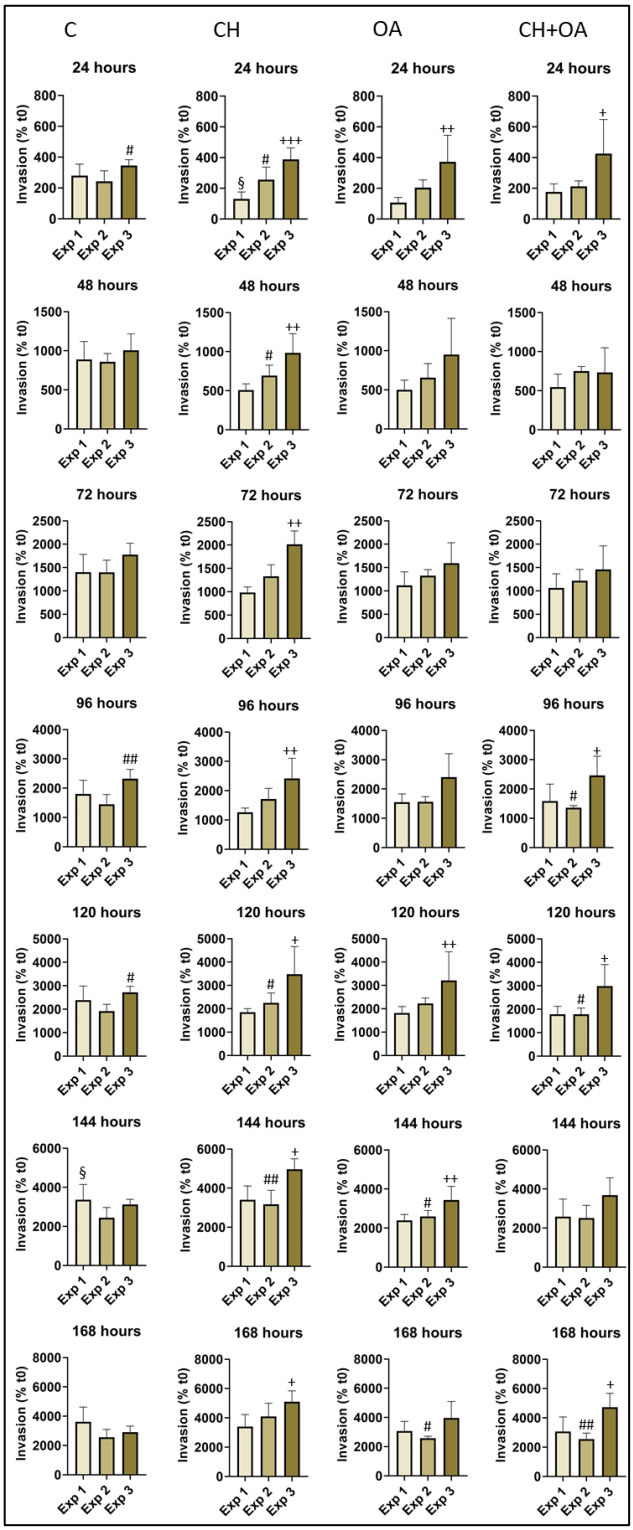

Fig. 6: Observed variations in the invasion activity of OSCA40 spheroids between the exp 1, exp 2 and exp 3 for each treatment group (CH, OA, CH + OA, C) during 168 hours analyses in the 3D invasion assay. The results represent the mean ± standard deviation. §$p<0.05$ in relation Exp 1 vs. Exp 2; +$p<0.05$, ++$p<0.01$, +++$p<0.001$ in relation Exp 1 vs. Exp 3; #$p<0.05$, ##$p<0.01$ in relation Exp 2 vs. Exp 3.

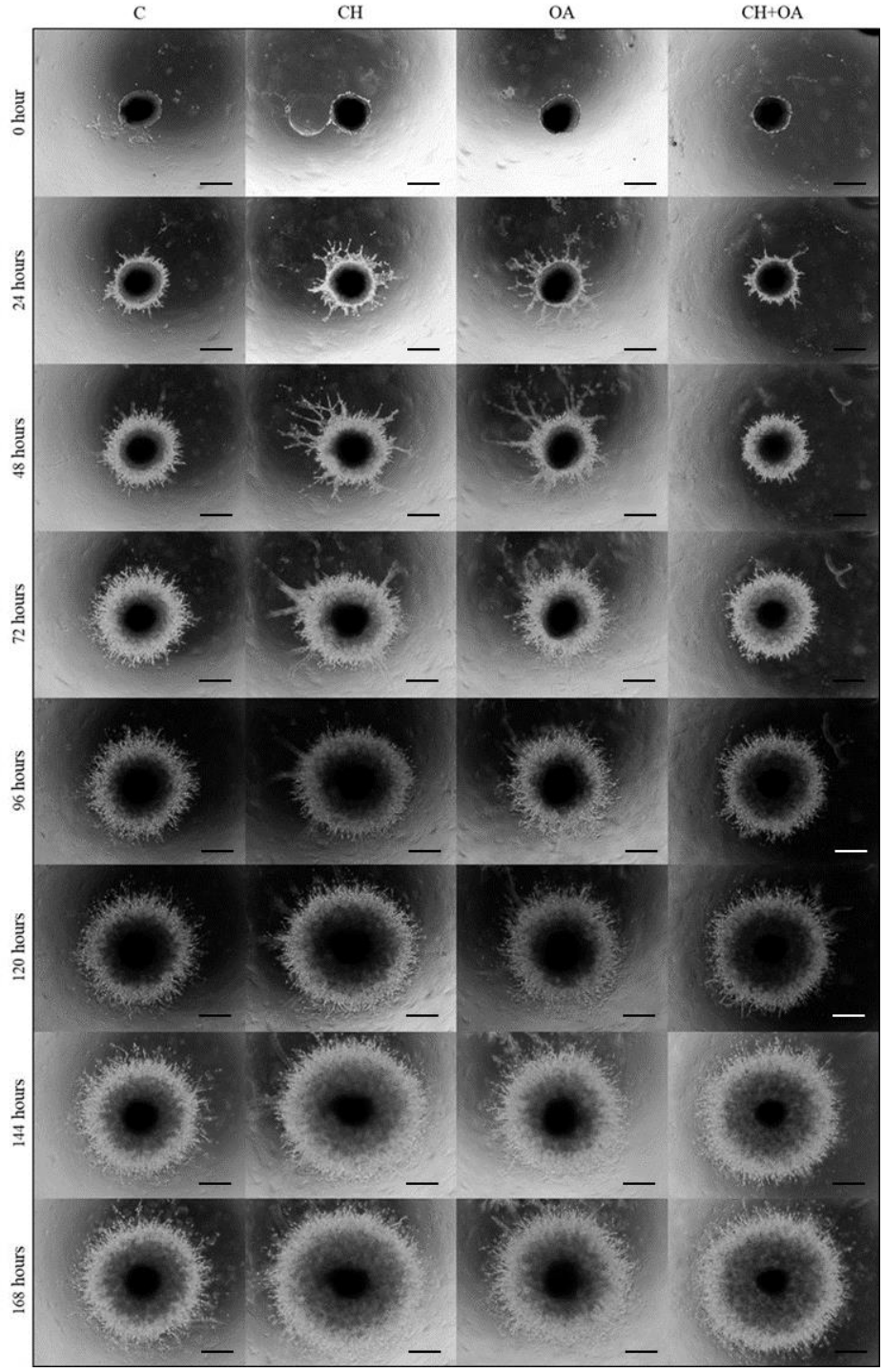

Fig. 7: Selection of microphotographs representing the OSCA40 spheroids 3D invasion assay. The spheroids were stimulated with CH, OA, CH + OA with the concentrations 4 µl/ml, 0,1 µl/ml, 4 µl/ml + 0,1 µl/ml, respectively, and C incubated with standard medium. The images were taken using a 4x magnification, detecting the development of the invadopodia through the 168 hours of the experiment. The 0-hour image is used for relative invasion calculation (scale = 500 µm).

3.3 qRT-PCR

The figure 8 shows the results obtained in relation to the gene expression in OSCA40 spheroids for PLIN1, PLIN2, PLIN3, PLIN4, PLIN5, ABCA1, GAPT3, GSK3B, MGLL, MYC, PLPP2, ORL1, SCARB2, SREBF1 and USF2. The presented fold change is related to the untreated C group. The analyses were made comparing groups stimulated with CH, OA and CH+ OA to C. We observed a decrease in ABCA1 expression of OSCA40 spheroids stimulated with CH+ OA ($p<0.05$) in relation to C. We also observed a decrease in SREBF1 expression of OSCA40 spheroids stimulated with CH ($p<0.0001$) and CH+ OA ($p<0.05$) in relation to C.

It wasn´t possible to measure the ORL1 and PLIN5 gene expression, the samples didn´t produce a Ct value, necessary for the calculations.

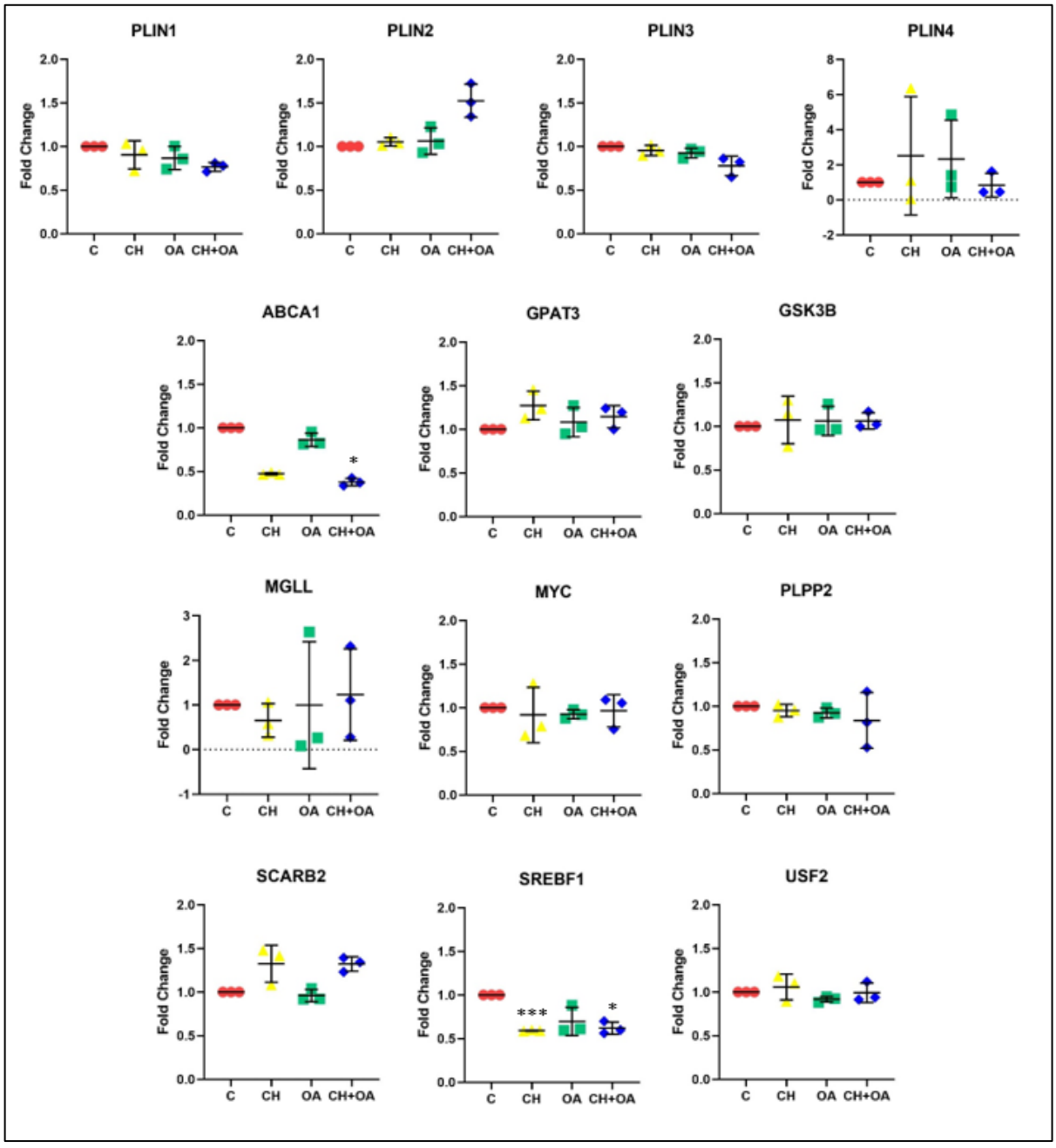

Fig. 8: Detection of genes of interest for osteosarcoma development and spread, under the effects of CH, OA, CH + OA and C. The gene expression level in OSCA40 spheroids is presented as fold change relative to the C of each tested gene, the increase or decrease in gene expression level is in relation to the C. The results represent the mean ± standard deviation of three independent experiments. *p<0.05, ***p<0.001 in relation to C.

3.4 Immunohistochemistry

The figure 9 shows the results obtained in relation to the Ki67 protein detection of OSCA40 spheroids for each experiment. The figure 10 shows the results obtained in relation to the Ki67 protein detection of OSCA40 spheroids for each treatment.

The exp 1 and the exp 2 showed no increase or decrease in the Ki67 protein detection of OSCA40 spheroids stimulated with CH, OA, CH + OA in relation to C ($p>0.05$). The exp 3 showed a decrease in the Ki67 protein detection of OSCA40 spheroids stimulated with CH + OA in relation to C ($p<0.01$).

Also, when comparing the different experiments with each other, we observed a variation in the Ki67 protein detection of OSCA40 spheroids in the presence of CH, OA, CH + OA, C ($p <0.05$). The exp 1, exp 2 and exp 3 showed no increase or decrease in the Ki67 protein detection of OSCA40 spheroids in relation to each other stimulated with CH and C ($p>0.05$). The exp 2 showed an increase in the Ki67 protein detection of OSCA40 spheroids in relation to the exp 1 stimulated with OA ($p<0.05$). The exp 2 showed an increase in the Ki67 protein detection of OSCA40 spheroids in relation to the exp 1 ($p<0.05$) and to the exp 3 ($p<0.01$) stimulated with CH + OA.

The figure 11 shows the results obtained in relation to the H&E and Ki67 immunohistochemical staining of OSCA40 spheroids stimulated with CH, OA, CH + OA and C. For the morphology of spheroids stained with H&E, we observed the presence of diffuse proliferation of small to medium sized cells. Medium cells are located in the peripheric region. Small cells with reduced cytoplasm, having round or some oval hyperchromatic nucleus, are present in the central region. Cells with pyknotic nucleus are present in intermediary region. The treatment with CH and CH + OA had a negative effect on cells morphology, increasing the necrotic areas and apoptotic bodies, localized mostly in central region. Spheroids treated with CH and CH + OA also have reduced cell cohesion. For the group treated with OA, central and intermediary regions presented necrotic areas. It was also observed mitotic figures in intermediary region in the spheroids treated with CH + OA.

The immunopositivity was visible as brown precipitate, being nuclear or cytoplasmic localized. The Ki67 stained the cell nucleus. The C and CH treated groups presented Ki67 distributed mostly in the peripheric and intermediary regions, while the spheroids treated with OA and CH

+ OA presented a homogenous distribution of Ki67 between peripheric, intermediary and central regions. All the groups presented a high concentration of Ki67

Figure 12 shows the results obtained in relation to the PLIN1, PLIN2, PLIN3, PLIN5 immunohistochemical staining of OSCA40 spheroids stimulated with CH, OA, CH + OA and C. Figure 13 shows the results obtained in relation to the PLIN1, PLIN2, PLIN3, PLIN5 immunohistochemical staining of C+ and C- cells. For the PLIN1, PLIN2, PLIN3 and PLIN5 staining we observed variations. The PLIN1 was not detected in the spheroids treated with CH, OA, CH + OA and C. The PLIN2 was detected encircling lipid droplet in the cytoplasm of the cells. The spheroids treated with CH and C presented PLIN2 mostly in intermediary region, visible in some peripheric regions. The spheroids treated with OA and CH + OA presented PLIN2 mostly in peripheric region. The PLIN3 was detected in the cytoplasm of the cells. The spheroids treated with CH, OA, CH + OA and C presented PLIN3 homogeneously distributed in peripheric, intermediary and central area. The PLIN5 was detected mainly in the nucleus of the cells. The spheroids treated with CH, OA, CH + OA and C presented PLIN5 distributed in central area.

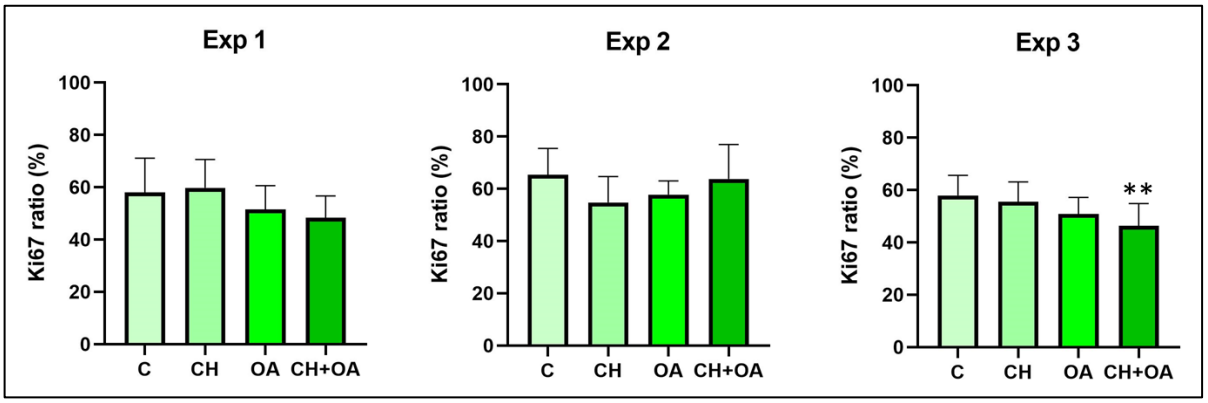

Fig. 9: Percentage of anti-Ki67 positive OSCA40 spheroids detected by means of immunohistochemistry within the spheroids stimulated with CH, OA, CH + OA and C in the concentrations 4 µl/ml, 0,1 µl/ml, 4 µl/ml + 0,1 µl/ml and only standard medium, respectively. The Ki67 ratio is the proportion of the detected Ki67 stained cells in the total number of cell nucleus. Three independent experiments were performed and their results are presented as mean ± standard deviation. **p<0.01 in relation to C.

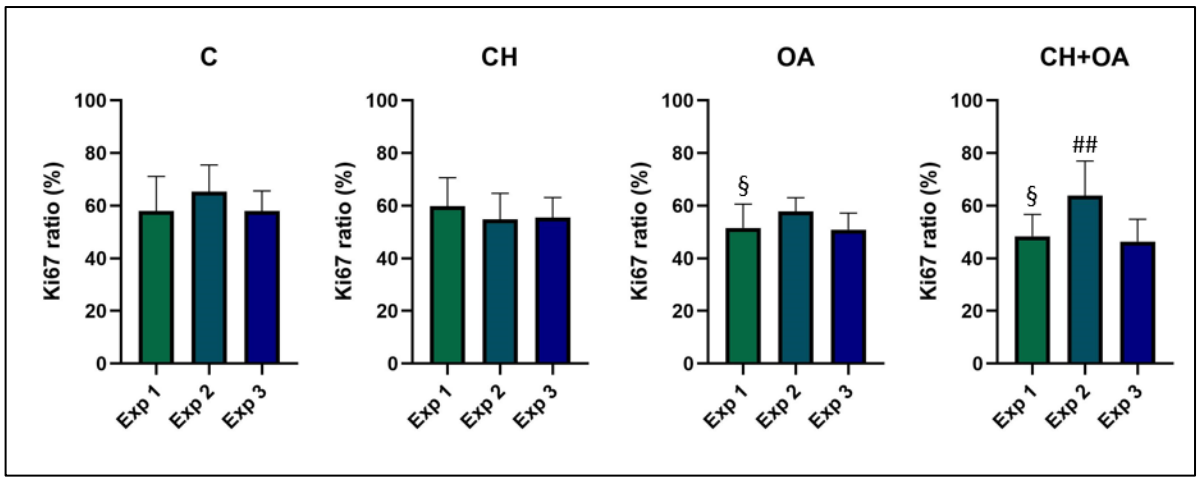

Fig. 10: Variations in the Ki67 detection in OSCA40 spheroids treated with CH, OA, CH+ OA and C in three independent experiments (exp 1, exp 2, exp 3), demonstrating the differences in the proliferation marker Ki67 between the experiments for each treatment. All the experiments were stimulated with the 4 different treatments and had the IHC staining following the same protocol. The results represent the mean ± standard deviation. Exp 1 vs. exp 2 §p<0.05; exp 2 vs. exp 3 ##p<0.01.

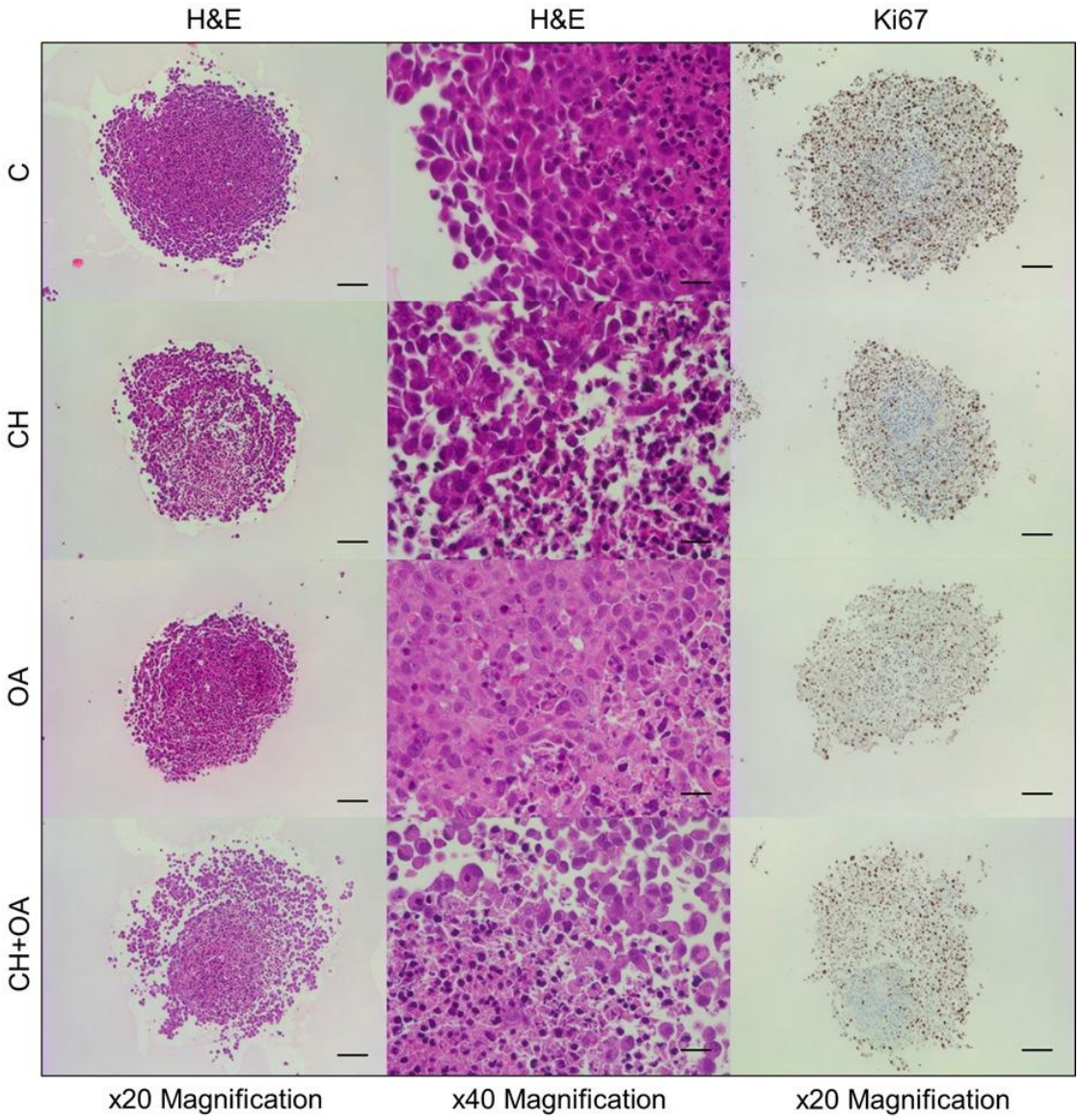

Fig. 11: Morphological alterations observed in the spheroids stained with H&E and immunohistochemical detection of Ki67 protein as proliferation marker within the C and the respective treatment groups: CH, OA and CH + OA. A x20 magnification was used to demonstrate spheroidal morphology and overall localization of Ki67 protein within the spheroids and x40 magnification was applied to demonstrate cellular morphology (scale x20 magnification = 100 µm; scale x40 magnification = 50 µm).

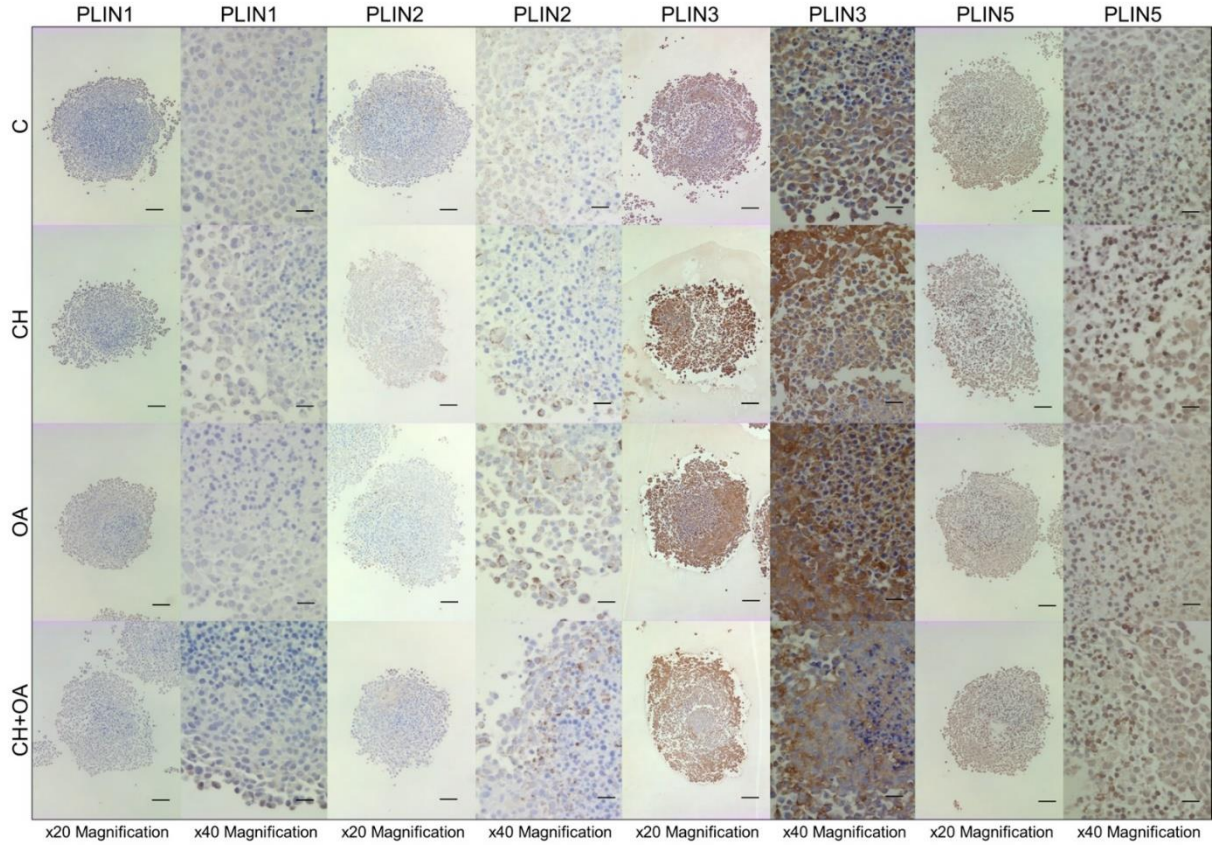

Fig. 12: PLIN1, PLIN2, PLIN3 and PLIN5 of the C and the respective treatment groups: CH, OA and CH + OA. A x20 magnification was used to demonstrate overall localization of the respective PLIN within the spheroids and x40 magnification was applied to demonstrate PLINs expression in cellular level (scale x20 magnification = 100 µm; scale x40 magnification = 50 µm).

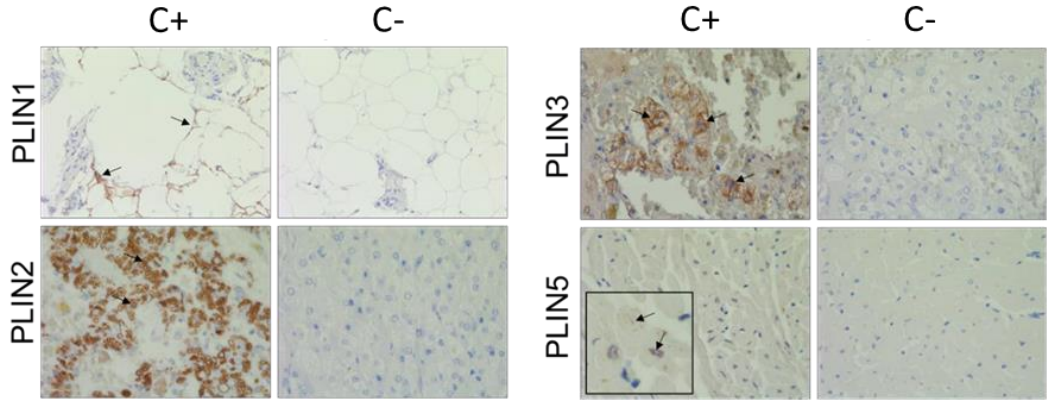

Fig. 13: Detection of the four members of the PLIN family of interest in canine FFPE tissue samples that served as C+. PLIN1 adipose tissue (arrows indicate the membranes of the adipocytes positive for PLIN1), PLIN2 adrenal gland Zona fasciculata (arrows indicate PLIN2 positive LDs in the endocrine cells), PLIN3 adrenal gland Zona arcuata (arrows indicate PLIN3 positive LDs in the endocrine cells), PLIN5 heart muscle (arrows indicate small LDs positive for PLIN5 between the intracellular filaments but also in the perinuclear zone).

3.5 Western blot

The figure 14 shows the results obtained in relation to the protein measurement of OSCA40 spheroids for PLIN2 and PLIN3, stimulated with CH, OA, CH + OA in relation to C. Figure 15 shows the results obtained in relation to the protein measurement of OSCA40 spheroids for PLIN2 and PLIN3, stimulated with CH, OA, CH + OA and C in the agarose gel. Figure 16 shows the results obtained in relation to the PLIN1, PLIN2, PLIN3, PLIN5 C+ and C- in comparison to the spheroids treated with CH, OA, CH + OA and C.

Semiquantitave analysis of the specific bands was performed and the bands present numerical values that are relative to the reference band for each sample. The experiment showed no increase or decrease in the protein content of OSCA40 spheroids stimulated with CH, OA, CH + OA in relation to C ($p>0.05$).

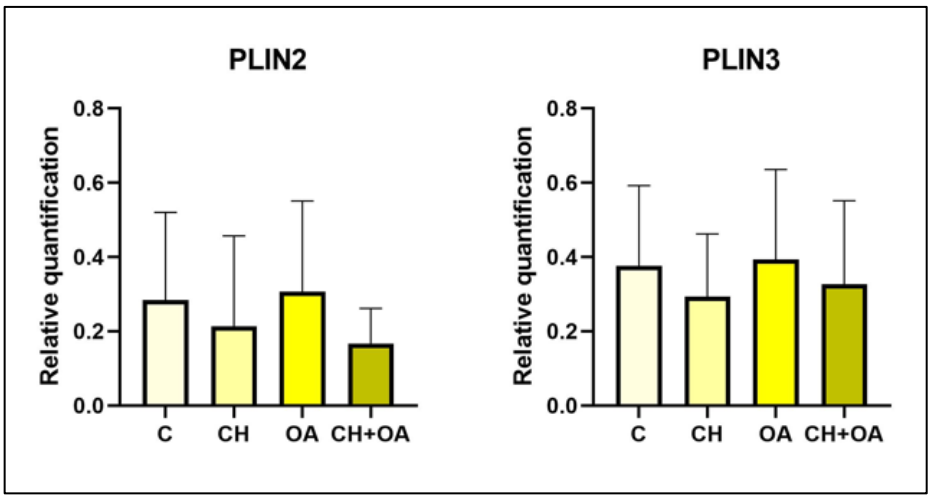

Fig. 14: Variation in PLIN2 and PLIN3 detection in OSCA40 spheroids stimulated with the treatments CH, OA, CH+ OA and C by means of WB. The concentration of protein was quantified relative to the reference band for each sample. The results represent the mean ± standard deviation of three independent experiments. * $p>0.05$ in relation to C.

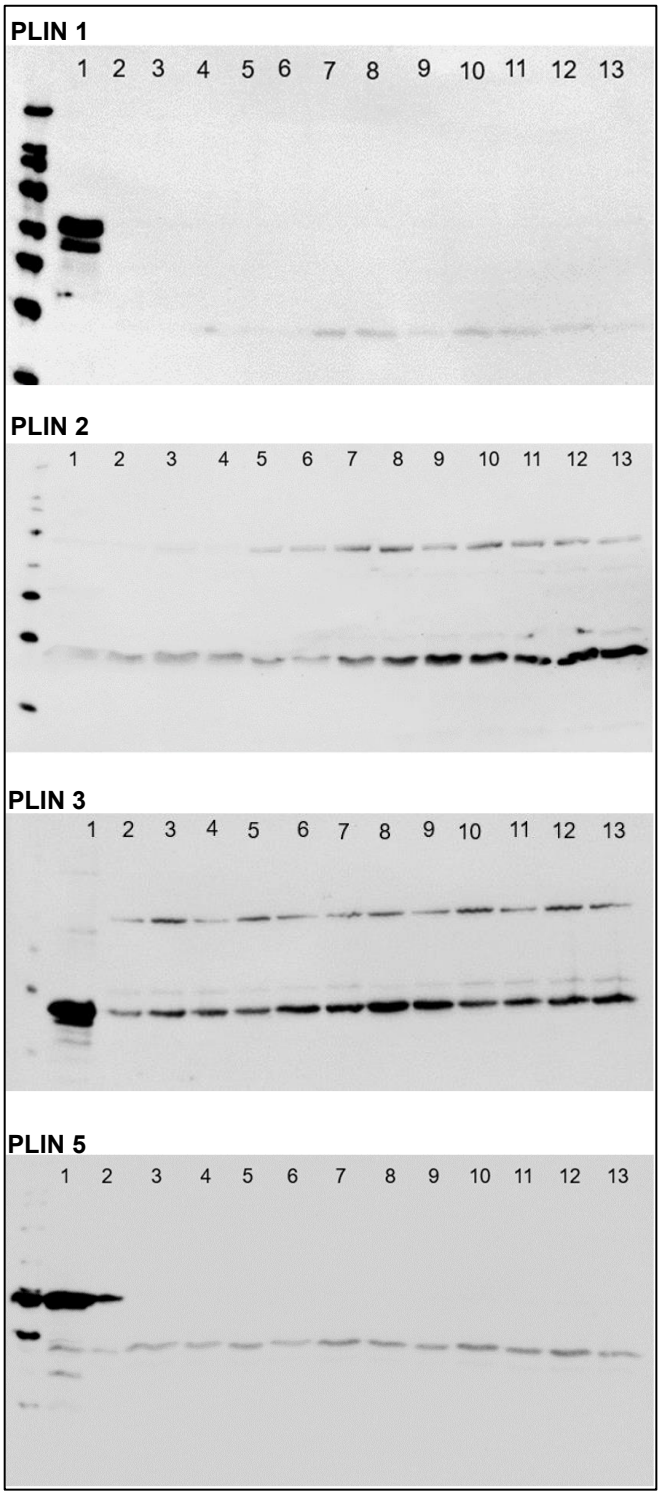

Fig. 15: Representation of PLIN1, PLIN2, PLIN3 and PLIN5 detection in OSCA40 spheroids by means of WB analysis. C+ for each member of the PLIN family are represented by lane 1 (PLIN1 canine adipose tissue; PLIN2 canine adrenal gland; PLIN3 canine skeletal muscle; PLIN5 canine heart muscle). Lanes 2-5 represent respectively C, OA, CH, CH + OA of exp 1. Lanes 6-9 represent respectively C, OA, CH, CH + OA of exp 2. Lanes 10-13 represent respectively C, OA, CH, CH + OA of exp 3.

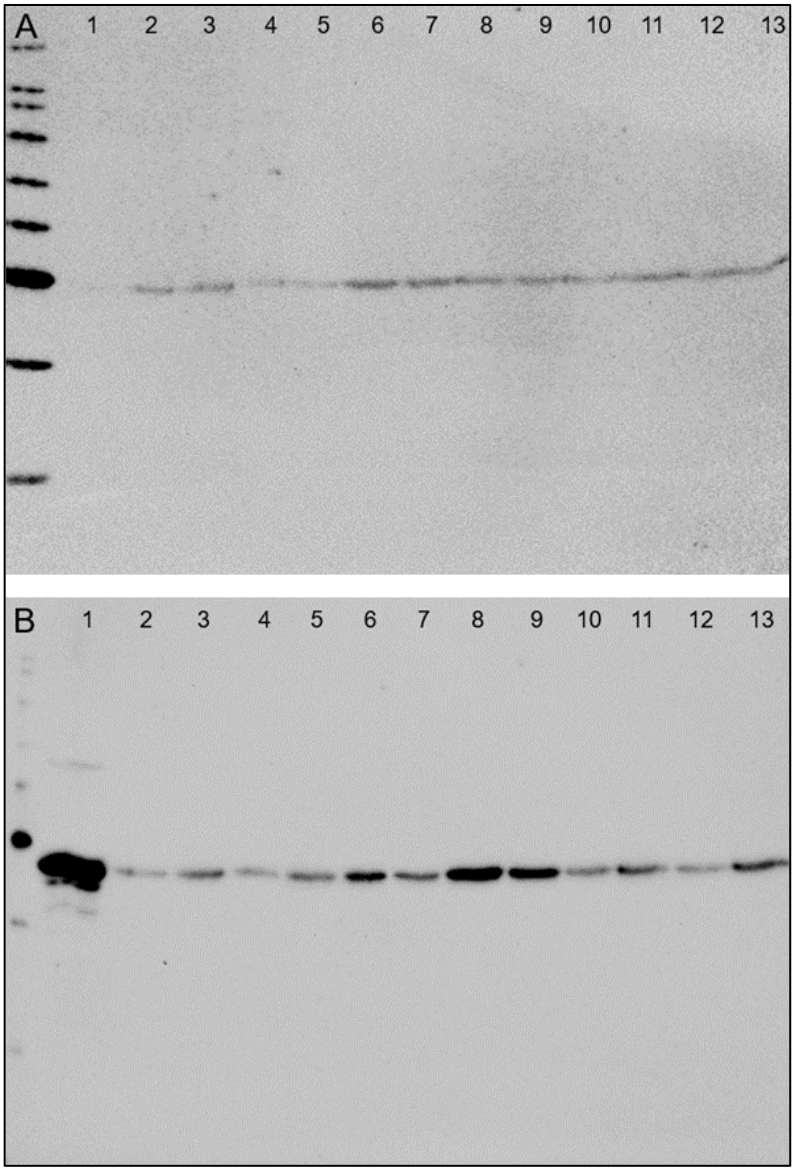

Fig. 16: C- are demonstrated in section A and B, having in section A lane 1 representing canine adipose tissue, the C+, C- for anti-rabbit secondary system; and in section B, having the lane 1 representing canine skeletal muscle, the C+, C- for anti-mouse secondary system. For both section A and B, the lanes 2-5 represent respectively C, OA, CH, CH + OA of exp 1. Lanes 6-9 represent respectively C, OA, CH, CH + OA of exp 2. Lanes 10-13 represent respectively C, OA, CH, CH + OA of exp 3.

4 Discussion

Osteosarcoma is the most common primary bone cancer in humans and dogs, and in both species the prognosis is worse in case of metastatic disease (Simpson, et al., 2017). Although chemotherapy and surgical excision can be used for the treatment, the low survival rate makes it fundamental to develop new treatments using different targets. The *in vitro* models are extremely important, making it possible to simulate a *in vivo* situation without experimenting in living beings the tested technics.

In our study we performed 2D and 3D invasion assays *in vitro*. The 2D assay is a faster and simpler technic to evaluate the cell invasion capacity but has its limitations since it works with a cell monolayer. The 3D assay provides a microenvironment closer to the *in vivo* situation, having also demonstrating the invadopodia formation, but it is more time and cost consuming and there is a broad range of difficulties in performing and analyzing the complex assay leading to the observed inter-experimental differences.

It has been demonstrated that lipids are part of the protein signaling in the membrane and cellular homeostasis, and that alterations in lipid metabolism can lead to immune disorders and cancer. It is also important to mention that CH metabolism upregulation have been observed in cancer. This adaptation is important to maintain the cancer cell constant proliferation (Roy, Dibaeinia, Fan, Sinha, & Das, 2019). The dynamics of intracellular lipid droplet formation, storage and lipid metabolism is closely intertwined with surface proteins of the lipid droplets. These proteins are classified in structure proteins, such as PLINs, membrane-trafficking proteins, and enzymes implicated in lipid synthesis and catabolism (Tirinato, et al., 2017).

Overexpression of members of PLINs, a family of lipid droplet coating protein, was observed in cancer cells promoting accumulation of lipid droplets (Diao & Lin, 2019). It has been shown that silencing PLIN2 attenuates the growth of tumor cells and that the higher expression of PLIN2 is suggested to be protective against lipotoxicity (Khor, Shen, & Kraemer, 2013).

The experiment performed by Makino, et al., 2016 demonstrated that free CH accumulation induces the degradation of PLIN2. They performed tests loading free CH into cultured hepatocytes, observing also the fusion of lipid droplets, lipid droplets enlargement and fusion of lipid droplets to the endoplasmic reticulum (Makino, et al., 2016).

Additionally, according to Shyu Jr, et al., 2018, 'therapy-induced senescence' cells demonstrated that excess lipids that could not be stored in overloaded lipid droplets may promote lipotoxic diacylglycerol and ceramides causing stress-induced cellular senescence. Having in mind that the excessive storage of lipid droplets has a potential to cause remission inducing senescence in cells (Shyu Jr, Wong, Crasta, & Thibault, 2018), we interpreted our results considering also the possible inhibitory effects of the lipids.

Different methods can be used to investigate osteosarcoma pathogenesis and progression *in vitro*. As invasion of osteosarcoma is a very important event to investigate the invasive capacity of the cells and to identify their potential for metastatic spread, an invasion assay is an important tool for *in vitro* analysis of osteosarcoma cells and potential therapeutic targets and approaches (De Luca, et al., 2018). The 2D invasion assay applied in the present study enables to monitor invasion through an extracellular matrix that mimics the natural composition of basement membranes, a process that is observed in cancer metastasis.

We used this method to observe the invasive capacity, but the cancer cell potential can be reduced using a monolayer because the cell-cell and cell-matrix interactions are missing. Therefore, the data obtained from the 2D cell culture is less reliable because the cell monolayer does not reflect the real three-dimensional tumor microenvironment. Unfortunately, this method does not represent the tumor cell biology, the macrostructure, complexity and variations of the tumor microenvironment. Although the 2D invasion assay has limitations, it is an accessible cell migration assay and useful for many biological studies (Justus, Leffler, Ruiz-Echevarria, & Yang, 2014).

Our tests showed that in the exp 1 there was an increase in the cell invasion of the cells treated with CH compared with C ($p<0.05$) and the exp 2 showed an increase in the cell invasion of the cells treated with CH + OA compared with C ($p<0.05$). We also observed many variations between the three experiments, making the observed increase in the cell invasion not significant. It would be necessary to perform more repetitions to rule out the experiments' variations as a factor influencing the cell invasion we observed. Another possibility are errors during the preparation, causing the evident variations between the tests. In this case more repetitions would also help to standardize the methods and the equipment manipulation to avoid those variations and errors.

The test also showed that the different cell treatments caused an increase in the cells' invasion, indicating that the provided lipids actually worked in a pro-tumorigenic direction, providing substrate for the cancer cells upregulated metabolism instead inhibiting. We question if the concentration of lipids could be a factor. In the future the test could be done providing different concentrations of lipids to observe if there is a threshold when the lipids start acting in an inhibitory way, due to lipotoxicity or degradation of PLIN2. More tests should be performed also to have more samples, which would give our test a bigger power of prediction, representing more accurately the possible variations observed.

We performed one more method to observe the cell invasion capacity, this time using a 3D cell model, which does not represent in a realistic way the complexity and heterogeneity of osteosarcoma but simulates better the microenvironmental physiology of tumors (De Luca, et al., 2018). The method with scaffold (Matrigel) was chosen, having a basement membrane to support the spheroid and to represent the barriers invaded by metastatic tumor cells (Trevigen, Inc, 2016). *In vitro* assays are important models to extrapolate to *in vivo* situations and study live cells behavior, like the invasion metastatic properties of cancer cells (Pijuan, et al., 2019). This model also made it possible to observe the invadopodia, present during a malignant progression, important for tumor cell invasion and dissemination (Vinci, Box, & Eccles, 2015). Studying the invasive capacity of osteosarcomas, this is an important factor to consider. This structure and its progression can only be observed in a 3D cell culture model.

The cellular metabolic state of a cell is influenced by the size and amount of lipid droplets, also by their composition. Lipid droplets i*n vitro* are influenced by the culture conditions, while the cells *in vivo* have the interference of other factors as resting, fasting, and pathological status (Tirinato, et al., 2017). The microenvironment is fundamental for the cancer cells' development, for instance significant amount of CH in tumor tissue is derived from dietary CH that is imported from adipocytes in the tumor microenvironment (Roy, Dibaeinia, Fan, Sinha, & Das, 2019), being important to apply models closer the reality.

Our 3D invasion assay results have shown that only the exp 1 had differences in the invasion of the treated spheroids compared to C in the first 72 hours. The time 24 hours showed a decrease of invasion of spheroids treated with CH ($p<0.001$), OA ($p<0.001$) and CH + OA ($p<0.01$) compared to C. The time 48 hours showed a decrease of invasion of spheroids treated with CH ($p<0.01$), OA ($p<0.01$) and CH + OA ($p<0.01$) compared to C. The time 72 hours

showed a decrease of invasion of spheroids treated with CH ($p<0.05$) compared to C. These observations can be result of the high amount of lipids covering the spheroids during the initial hours, taking a longer time until those spheroids can break this lipidic barrier around them. Another possibility is that spheroids were trying to adapt the lipid droplets to the exogenous lipids, causing the slower growth during the initial hours.

Exp 2 and exp 3 presented a variation in the cell invasion in the last hours. Exp 2 has shown an increase of invasion in spheroids treated with CH ($p<0.01$) compared to C at 168 hours. Exp 3 has shown an increase of invasion in spheroids treated with CH ($p<0.01$) compared to C at 144 hours and an increase of invasion in spheroids treated with CH ($p<0.0001$), OA ($p<0.05$) and CH + OA ($p<0.0001$) compared to C at 168 hours. These observations can be caused by the technical limitation of the test. The assay may be conducted for longer periods if desired but the limitation is when the structure size begins to exceed the field of analysis or the spheroids begin to expire. The spheroids observed on time 144 hours and 168 hours were too big to be captured in the microscope field, causing measurement errors when analyzed, probably generating the invasion variation.

When comparing the different experiments for each treatment we observed many variations, being questionable if the observed variations in invasion of the treated groups compared to the C a representative. Once again, performing more test would be fundamental to verify if the observed variations are cause by technical difficulties or if there is a real influence of the treatments on the cell invasion. Also, in this test would be important to test different concentrations of lipid to identify a possible threshold between promoting and inhibiting the cell invasion. Performing more tests would also help to improve the technic used and reduce the human errors. It is always important to mention that more tests would increase the power of prediction of our analyses and its representativity.

The treated spheroids presented a variation during the initial hours, decreasing the invasion compared to the C, but the final hours showed again an increase in invasion compared to the C. It is indicative that the spheroids initially were adapting to the lipids surrounding them, possibly having no effect or promoting the cell invasion in the next hours of the experiment. There isn't much information available about how long a 3D invasion assay should be performed, with our study we demonstrated that the period of observation should be limited by the technical capacity of the equipment used for the analyses, the measurements from 120, 144 and 168 hours

presented many variations, showing that for our equipment the analyses present a better result until 96 hours.

According to Roy et. al., 2019, cancer cells have a differentiated expression and mutations of genes involved with the CH homeostasis. Those variations include increases in gene copy numbers, upregulation of CH synthesis gene expression, increased CH import by LDL receptors, and decreased transport of CH. As lipid droplets possibly participate enhancing cancer aggressiveness, it makes the lipid droplets and the mechanisms involved in their metabolism a promising target for cancer therapy (Shyu Jr, Wong, Crasta, & Thibault, 2018).

The qRT-PCR analyses have shown a variation of gene expression in the treated spheroids compared with the C in only two genes, ABCA1 and SREBF1. For the gene ABCA1, the spheroids treated with CH + OA presented a decrease in gene expression compared to C ($p<0.05$). We believe that the observed decrease is caused by oncogenic mutation. Smith & Land, 2012, demonstrated that ABCA1 deficiency possibilists the increase of mitochondrial CH due to the defective CH efflux, inhibits release of mitochondrial cell death-promoting molecules, making possible the cancer cell survival, being an indicative that elevated mitochondrial CH is necessary for the cancer metabolism. This alteration shows that the treatment with CH + OA actually had a pro-tumorigenic effect, suppressing the gene expression to support the upregulated cancer cell metabolism.

For the gene SREBF1, the spheroids treated with CH ($p<0.0001$) and CH + OA ($p<0.05$) presented a decrease in gene expression compared to C. It has been demonstrated that the lack of PLIN1 resulted in decreased SREBP-1 activation, resulting in reduced SREBP-1 expression (Takahashi, et al., 2013). Itabe, et al., 2017, showed in his work that SREBP-1 is activated through the S1P-mediated proteolytic pathway in response to PLIN-induced lipid droplets generation in differentiating adipocytes. PLIN2 is present in immature preadipocytes, being replaced by PLIN1 in lipid-rich lipid droplets during differentiation into mature adipocytes. PLIN1 is abundantly expressed in mature adipocytes. As our canine osteosarcoma cells are not comparable with mature adipocytes, there was a lack of PLIN1 expression (even on protein levels), resulting in reduced in SREBF1 expression.

The genes OLR1 and PLIN5 did not produce a Ct value, not being possible to calculate the gene expression. It can be caused by an unsuited reference gene or if the amount of the RNA was too small to be amplified.

The results obtained from PLIN4 and MGLL gene expression are not reliable or representative, they are too close to the Ct detection limit. We also take in consideration that ORL1 and MGLL are very weekly expressed in the cell line we used, being questionable their representativity. For the genes PLIN4 and PLIN5 new primers could be tested and possible produce better readings.

The treatments didn't affect the expression of many genes, again we can question if the dose of lipids used is a reason, and if establishing a threshold for the treatments could provide a better scenario to compare the real effect of the treatments.

Osteosarcomas are characterized by a pleomorphic and heterogeneous microscopic appearance, apoptosis and necrosis are common in these tumors (Khor, Shen, & Kraemer, 2013). Other characteristic of the tumors can be assessed by detecting the proteins present in the cells. For examples, the Ki-67 protein is expressed during the proliferative phases of the cell, its detection helps to identify the growth fractions of tumors (Richardsen, et al., 2017). According to Li et al., 2015, tumors can be classified as low, intermediate, and highly proliferative, according to the Ki-67 index of ≤15 %, 16 %–30 %, and >30 %, respectively. Osteosarcoma is a highly proliferative cancer, all the treatment groups and C presented a proliferation ratio >40 % ($p<0,05$).

Our immunohistochemical analyses demonstrated that only the exp 3 featured differences in the Ki67 detection of the treated spheroids compared to the C. We observed a decrease in Ki67 detection of spheroids treated with CH + OA ($p<0.01$) compared to C. This result can indicate that the treatment could actually reduce the proliferation of cancer cells in presence of free lipids. Maybe the *in vitro* environment does not provide all the necessary components to represent the *in vivo* situation. As the alteration occurred only in one experiment, there is also the possibility that the variation was caused by a counting or any technical error. New tests should be performed to investigate if the observed result is representative or if it was a technical error.

Our tests presented variations between the experiments when analyzed for each treatment. We observed an increase in the Ki67 detection of the spheroids treated with CH + OA in the exp 2 compared to the exp 1 ($p<0.05$) and the exp 3 ($p<0.01$). The results indicate that the observed variations are caused by technical errors, possibly the incorrect manipulation of the pipettes could cause the incubation of the cells with different lipid concentrations or to prepare spheroids

with different cell concentrations, generating those variations. Making new tests would clarify if the variations are expected or not, also practicing the manipulation of the laboratory equipment would help to avoid possible mistakes caused by pipetting.

The immunohistochemical staining did not detect the PLIN1 in the spheroids treated with CH, OA, CH + OA and C. It is reported that PLIN1 is abundantly expressed in mature adipocytes (Tirinato, et al., 2017), but as OSCA40 cells are not associated to adipocyte differentiation or white fat formation, the lack of PLIN1 expression on mRNA and protein levels was not surprisingly. In our tests we observed PLIN2 localized in lipid droplets, mostly in peripheric regions of the spheroids, probably because those areas are in direct contract with the medium containing the lipid treatments. It is demonstrated that PLIN2 is present in immature adipocytes and can be replaced by PLIN1 during differentiation into mature adipocytes (Itabe, Yamaguchi, Nimura, & Sasabe, 2017), therefore, it was possible that exogenous lipid stimulation might change the PLIN expression patterns in canine osteosarcoma cells *in vitro*. PLIN3 was detected in our tests distributed homogenously in the cytoplasm. Tirinato et al., 2017 observed that in the presence of adipogenic stimulus, PLIN3 and PLIN2 coat nascent lipid droplets. PLIN3 translocates from cytoplasm to nascent lipid droplet stimulating triacylglycerol biosynthesis and storage. The intense staining of PLIN3 in the immunohistochemical assays made it difficult to differentiate if there was abundant cytoplasmic staining or a lipid droplet associated localization of PLIN3 within the canine osteosarcoma cells. Furthermore, it was also possible, that the size of the PLIN3 positive lipid droplets was very small and thereby not visualized by light microscopy. To overcome these limitations a double-immunohistochemical approach staining PLIN2 and PLIN3 within one section would be possible. The combination of the two proteins allows to identify PLIN2 positive lipid droplets and a co-localization with PLIN3 could identify the structural relation of the two proteins of interest. Furthermore, confocal laser scanning microscopy would allow a higher and deeper resolution and could thereby visualize small lipid droplets which cannot be detected by light microscopy. Unfortunately, the two antibodies did not work in a combined approach for fluorescent immunohistochemistry. In future studies, different antibodies could be tested to find a potential combination of PLIN3 and PLIN2 detection within one section.

PLIN5 was detected mainly in the nucleus and the perinuclear cytoplasm. According to Gallardo-Montejano, et al., 2016, PLIN5 acts not only at the lipid droplet surface regulating

lipid storage, but also in the nucleus, as a transcriptional co-regulator that helps match mitochondrial capacity to the lipid load.

We performed WB analyses in our samples to allow semiquantitative analysis additional to immunohistochemical localization studies of the proteins of interest. We did not observe a significant increase or decrease in protein expression of PLIN2 and PLIN3 in the groups treated with CH, OA, CH + OA compared with C ($p<0.05$). The small number of our samples did not make it possible to analyze the differences between the groups. The results showed that the treatments did not interfere with the protein expression. New tests utilizing different concentrations of lipids might demonstrate if there is a threshold for the lipid concentration to interfered in the protein expression. Repeating the tests would also confirm that the treatments do not produce any alteration on the protein expression and rule out any possible technical interference. Our WB analysis was performed with a small number of samples, performing more tests would produce a more representative result. We also should consider to use a better-established protocol, in our test the C+ samples partially presented different molecular weight bands relative to the reference band.

Our tests did not detect the protein expression from PLIN1 and PLIN5. As mentioned before, PLIN1 probably wasn't detected because its expression occurs in mature adipocytes (Itabe, Yamaguchi, Nimura, & Sasabe, 2017) and our samples are in no way comparable in size, development or lipid content to a mature adipocyte, having PLIN2 displayed in our lipid droplets instead, as PLIN2 coats nascent lipid droplets and is positively correlated with the lipid droplet formation (Tirinato, et al., 2017). PLIN5 expression wasn't detected in our test, most likely because of its localization. PLIN5 not only operates in lipid droplets but also in the transcriptional regulation of mitochondrial respiration via nuclear translocation, PLIN5 is present in nuclear fractions (Gallardo-Montejano, et al., 2016). Possibly the lyse of our samples wasn't efficient enough to expose the cell nucleus, not being able the express the PLIN5 in our test. For the future tests, the samples preparation could be done applying a more efficient method, the material lyse can be done using bead beaters.

We can conclude with our present work that lipids are important for the cancer cells metabolism. PLIN1, PLIN2, PLIN3 and PLIN5 are involved with the tumor cell metabolism as well, acting in different locations and stages of the cell development. More tests are necessary to infer if and how exogenous lipids CH and OA modulate cancer cells, as our tests indicate a

pro-tumorigenic effect of lipids in OSCA40 cell *in vitro*. More experiments analyzing the influence of different concentrations of CH and OA can be valuable to define a threshold between promoting and inhibiting the cell invasion. The gene expression in cancer cells is regulated by a variety of factors, adapting to the different needs of the upregulated metabolism. Lipids are part of this regulatory system. We observed that performing different experiments can generate different outcomes instead of reliable repetitions. More tests should be performed to verify the assumptions and rule out the interferences.

5 References

Applied Biosystems. (2016). *High-Capacity cDNA Reverse Transcription Kits.* Foster City, USA: Pub. No. 4375222, Catalog Numbers 4368813, 4368814, 4374966, and 4374967.

Belisario, D. C., Akman, M., Godel, M., Campani, V., Patrizio, M. P., Scotti, L., . . . Riganti, C. (2020). ABCA1/ABCB1 Ratio Determines Chemo- and Immune-Sensitivity in Human Osteosarcoma. *Cells*, DOI 10.3390/cells9030647.

Bertolio, R., Napoletano, F., Mano, M., Maurer-Stroh, S., Fantuz, M., Zannini, A., . . . Sal, G. D. (2019). Sterol Regulatory Element Binding Protein 1 Couples Mechanical Cues and Lipid Metabolism. *Nat Commun*, 10(1):1326 DOI 10.1038/s41467-019-09152-7.

Carrillo, C., Cavia, M., & Alonso-Torre, S. (2012). Antitumor effect of oleic acid; mechanisms of action. A review. *Nutricion hospitalaria: organo oficial de la Sociedad Espanola de Nutricion Parenteral y Enteral*, 27(6):1860-5 DOI: 10.3305/nh.2012.27.6.6010.

Chen, N., Szentirmay, M. N., Pawar, S. A., Sirito, M., Wang, J., Wang, Z.-q., . . . Sawadogo, M. (2006). Tumor-suppression function of transcription factor USF2 in prostate carcinogenesis. *Oncogene*, 25(4):579-87 DOI 10.1038/sj.onc.1209079.

Crosby, K., Simendinger, J., Grange, C., Ferrante, M., Bernier, T., & Standen, C. (2020, 06 22). Immunohistochemistry Protocol for Paraffin-embedded Tissue Sections. Danvers,, MA, 01923, USA. Retrieved from https://www.jove.com/video/5064/immunohistochemistry-protocol-for-paraffin-embedded-tissue-sections

De Luca, A., Raimondi, L., Salamanna, F., Carina, V., Costa, V., Bellavia, D., . . . Giavaresi, G. (2018). Relevance of 3d culture systems to study osteosarcoma environment. *Journal of Experimental & Clinical Cancer Research*, 37:2 DOI 10.1186/s13046-017-0663-5.

Diao, X., & Lin, T. (2019). Progress in therapeutic strategies based on cancer lipid metabolism. *Thoracic Cancer*, DOI 10.1111/1759-7714.13146.

Ding, X., Zhang, W., Li, S., & Yang, H. (2019). The role of cholesterol metabolism in cancer. *Am J Cancer Res.*, 219-227 DOI 10.3389/fendo.2019.00690.

Duda, P., Akula, S. M., Abrams, S. L., Steelman, L. S., Martelli, A. M., Cocco, L., . . . A, J. (2020). Targeting GSK3 and Associated Signaling Pathways Involved in Cancer. *Cells*, 30;9(5):1110 DOI 10.3390/cells9051110.

Duraiyan, J., Govindarajan, R., Kaliyappan, K., & Palanisamy, M. (2012). Applications of immunohistochemistry. *J Pharm Bioallied Sci.*, 4(Suppl 2): S307–S309 DOI 10.4103/0975-7406.100281.

Foley, J. M., II, D. J., Monks, N. R., Cherba, D., Monsma, D. J., Davidson, P., . . . Steensma, M. R. (2015). Anoikis-resistant subpopulations of human osteosarcoma display significant chemoresistance and are sensitive to targeted epigenetic therapies predicted by expression profiling. *Journal of Translational Medicine*, DOI 10.1186/s12967-015-0466-4.

Gallardo-Montejano, V. I., Saxena, G., Kusminski, C. M., Yang, C., McAfee, J. L., Hahner, L., . . . Bickela, P. E. (2016). Nuclear Perilipin 5 integrates lipid droplet lipolysis with PGC-1α/SIRT1-dependent transcriptional regulation of mitochondrial function. *Nat Commun.*, 7: 12723 DOI 10.1038/ncomms12723.

Gebhard, C., Millerb, I., Hummel, K., Ondrovics, M. N., Schlosser, S., & Walter, I. (2018, April). Comparative proteome analysis of monolayer and spheroid culture of canine osteosarcoma cells. *Journal of Proteomics, 177*, 124-136 DOI 10.1016/j.jprot.2018.01.006.

Grabner, G. F., Zimmermann, R., Schicho, R., & Taschler, U. (2017). Monoglyceride lipase as a drug target: At the crossroads of arachidonic acid metabolism and endocannabinoid signaling. *Pharmacol Ther.*, 175: 35–46 DOI 10.1016/j.pharmthera.2017.02.033.

Han, G., Wang, Y., & Bi, W. (2012). C-Myc Overexpression Promotes Osteosarcoma Cell Invasion via Activation of MEK-ERK Pathway. *Oncology Research Featuring Preclinical and Clinical Cancer Therapeutics, 20*, 149-156 DOI 10.3727/096504012X13522227232237.

Heybrock, S., Kanerva, K., Meng, Y., Ing, C., Liang, A., Xiong, Z.-J., . . . Schwake, M. (2019). Lysosomal Integral Membrane protein-2 (LIMP-2/SCARB2) Is Involved in Lysosomal Cholesterol Export. *Nat Commun*, 6;10(1):3521 DOI 10.1038/s41467-019-11425-0.

Hoffman, B., & Liebermann, D. A. (1998). The proto-oncogene c-myc and apoptosis. *Oncogene*, 17,3351-3357 DOI 10.1038/sj.onc.1202592.

Itabe, H., Yamaguchi, T., Nimura, S., & Sasabe, N. (2017). Perilipins: a diversity of intracellular lipid droplet proteins. *Lipids in Health and Disease*, 83 DOI 10.1186/s12944-017-0473-y.

Jiang, L., Jiang, S., Zhou, W., Huang, J., Lin, Y., Long, H., & Luo, Q. (2019). Oxidized low density lipoprotein receptor 1 promotes lung metastases of osteosarcomas through regulating the epithelial-mesenchymal transition. *Journal of Translational Medicine*, DOI 10.1186/s12967-019-2107-9.

Jo, J., Choi, S., Oh, J., Lee, S.-G., Choi, S. Y., Kim, K. K., & Park, C. (2019). Conventionally used reference genes are not outstanding for normalization of gene expression in human cancer research. *BMC Bioinformatics*, 245 DOI 10.1186/s12859-019-2809-2.

Justus, C., Leffler, N., Ruiz-Echevarria, M., & Yang, L. (2014). *In vitro* Cell Migration and Invasion Assays. *Journal of Visualized Experiments 88(88)*, DOI 10.3791/51046.

Khor, V., Shen, W., & Kraemer, F. (2013). Lipid Droplet Metabolism. *Curr Opin Clin Nutr Metab Care.*, 16(6) 632-637 DOI 10.1097/MCO.0b013e3283651106.

Li, C., Yang, W., Zhang, J., Zheng, X., Yao, Y., Tu, K., & Liu, Q. (2014). SREBP-1 Has a Prognostic Role and Contributes to Invasion and Metastasis in Human Hepatocellular Carcinoma. *International Journal of Molecular Sciences*, 7124-7138 DOI 10.3390/ijms15057124.

Li, L. T., Jiang, G., Chen, Q., & Zheng, J. N. (2015). Ki67 Is a Promising Molecular Target in the Diagnosis of Cancer (Review). *Mol Med Rep.*, Mar;11(3):1566-72 DOI 10.3892/mmr.2014.2914.

Mahmood, T., & Yang, P.-C. (2012). Western Blot: Technique, Theory, and Trouble Shooting. *N Am J Med Sci.*, 4(9):429-34 DOI 10.4103/1947-2714.100998.

Makino, A., Hullin-Matsuda, F., Murate, M., Abe, M., Tomishige, N., Fukuda, M., . . . Kobayashia, T. (2016). Acute accumulation of free cholesterol induces the degradation of perilipin 2 and Rab18-dependent fusion of ER and lipid droplets in cultured human hepatocytes. *Mol Biol Cell.*, 27(21): 3293–3304 DOI 10.1091/mbc.E15-10-0730.

Marinho, L. C., Patrício, F. R., Filho, R. J.-G., Petrilli, A. S., Odashiro, L. N., Macedo, C., & Alves, M. T. (2005). Clinicopathologic study and Ki-67 proliferative marker evaluation in human osteosarcomas. *J. Bras. Patol. Med. Lab.*, vol.41 no.6 DOI 10.1590/S1676-24442005000600008 .

Medicine, U. N. (2020, 06 22). *OAZ1 ornithine decarboxylase antizyme 1 [Homo sapiens (human)]*. Retrieved from National Center for Biotechnology Information: https://www.ncbi.nlm.nih.gov/gene/4946

Medicine, U. N. (2020, 06 22). *RPL27 ribosomal protein L27 [Homo sapiens (human)]*. Retrieved from National Center for Biotechnology Information: https://www.ncbi.nlm.nih.gov/gene/6155

Mulisch, M., & Welsch, U. (2010). *Romeis - Mikroskopische Technik* (18th ed.). Heidelberg: Spektrum Akademischer Verlag.

Pijuan, J., Barcelo, C., Moreno, D., Maiques, O., Siso, P., Marti, R., . . . Panosa, A. (2019). Front Cell Dev Biol. 7:107. In vitro Cell Migration, Invasion, and Adhesion Assays: From Cell Imaging to Data Analysis, DOI 10.3389/fcell.2019.00107.

Qyang, Y., Luo, X., Lu, T., Ismail, P. M., Krylov, D., Vinson, C., & Sawadogo1, M. (1999). Cell-Type-Dependent Activity of the Ubiquitous Transcription Factor USF in Cellular Proliferation and Transcriptional Activation. *Molecular and Cellular Biology*, 1508–1517 DOI 10.1128/mcb.19.2.1508.

Richardsen, E., Andersen, S., Al-Saad, S., Rakaee, M., Nordby, Y., Pedersen, M. I., . . . Busund, L.-T. (2017). Evaluation of the proliferation marker Ki-67 in a large prostatectomy cohort. *PLoS One.*, 12(11): e0186852 DOI 10.1371/journal.pone.0186852.

Roy, J., Dibaeinia, P., Fan, T., Sinha, S., & Das, A. (2019). Global Analysis of Osteosarcoma Lipidomes Reveal Altered Lipid Profiles in Metastatic Versus Nonmetastatic Cells. *J Lipid Res.*, 60(2): 375-387 DOI 10.1194/jlr.M088559.

Shimozaki, S., Yamamoto, N., Domoto, T., Nishida, H., Hayashi, K., Kimura, H., . . . Tsuchiya, H. (2016). Efficacy of glycogen synthase kinase-3β targeting against osteosarcoma via activation of β-catenin. *Oncotarget*, DOI 10.18632/oncotarget.12781.

Shyu Jr, P., Wong, X., Crasta, K., & Thibault, G. (2018). Dropping in on Lipid Droplets: Insights Into Cellular Stress and Cancer. *Biosci Rep.*, 19;38(5) DOI 10.1042/BSR20180764.

Simpson, S., Dunning, M., de Brot, S., Grau-Roma, L., Mongan, N., & Rutland, C. (2017). Comparative review of human and canine osteosarcoma: morphology, epidemiology, prognosis, treatment and genetics. *Acta Vet Scand.*, 59: 71 DOI 10.1186/s13028-017-0341-9.

Smith, B., & Land, H. (2012). Anti-cancer activity of the cholesterol exporter ABCA1 gene. *Cell Rep.*, Sep 27; 2(3): 580–590. DOI 10.1016/j.celrep.2012.08.011.

Smith, C. J., & Osborn, A. M. (2009). Advantages and limitations of quantitative PCR (Q-PCR)-based approaches in microbial ecology. *FEMS Microbiology Ecology*, 67(1):6-20 DOI 10.1111/j.1574-6941.2008.00629.x.

Takahashi, Y., Shinoda, A., Furuya, N., Harada, E., Arimura, N., Ichi, I., . . . Sato, R. (2013). Perilipin-mediated Lipid Droplet Formation in Adipocytes Promotes Sterol Regulatory

Element-Binding protein-1 Processing and Triacylglyceride Accumulation. *PLoS One.*, May 29;8(5):e64605. DOI 10.1371/journal.pone.0064605.

Tang, X., Benesch, M. G., & Brindley, D. N. (2015). Lipid phosphate phosphatases and their roles in mammalian physiology and pathology. *The Journal of Lipid Research*, 2048-2060 DOI 10.1194/jlr.R058362.

Tirinato, L., Pagliari, F., Limongi, T., Marini, M., Falqui, A., Seco, J., . . . Di Fabrizio, E. (2017). An Overview of Lipid Droplets in Cancer and Cancer Stem Cells. *Stem Cells Int.*, DOI 10.1155/2017/1656053.

Trevigen, Inc. (2016). *Cultrex 3-D Spheroid Basement Membrane Extract Cell Invasion Assay, 96-well.* Maryland USA: Catalog #: 3500-096-K.

U.S. National Library of Medicine. (2020, 06 22). *OLR1 oxidized low density lipoprotein receptor 1 [Homo sapiens (human)]*. Retrieved from National Center for Biotechnology Information: https://www.ncbi.nlm.nih.gov/gene/4973

U.S. National Library of Medicine. (2020, 06 22). *USF2 upstream transcription factor 2, c-fos interacting [Homo sapiens (human)]*. Retrieved from National Center for Biotechnology Information: https://www.ncbi.nlm.nih.gov/gene/7392

Vinci, M., Box, C., & Eccles, S. (2015). Three-Dimensional (3D) Tumor Spheroid Invasion Assay. *J Vis Exp. (99): 52686*, DOI 10.3791/52686.

Wang, N., Silver, D. L., Thiele, C., & Tall, A. R. (2001). ATP-binding Cassette Transporter A1 (ABCA1) Functions as a Cholesterol Efflux Regulatory Protein. *Journal of Biological Chemistry*, 276(26):23742-7 DOI 10.1074/jbc.M102348200.

Wolfe, T. D., Pillai, S. P., III, B. E., Lanigan, L. G., Martin, C. K., Werbeck, J. L., & Rosol, T. J. (2011, April). Effect of zoledronic acid and amputation on bone invasion and lung metastasis of canine osteosarcoma in nude mice. *Clin Exp Metastasis*, 377–389 DOI 10.1007/s10585-011-9377-9.

Zymo Research Corp. (n.d.). *Direct-zol™ RNA MiniPrep.* Irvine, USA: Catalog Nos. R2050, R2051, R2052, R2053.

6 Abstract

Osteosarcomas are the most common type of bone cancer, highly aggressive and frequently spread to lungs and other bones in metastatic disease. Alterations in lipid metabolism can be related to cancer, since lipids are necessary for cancer cells as energy storage and signaling pathway. Lipid droplets participate in the lipid accumulation and metabolism. Perilipins (PLINs) proteins coat the lipid droplets, controlling the cellular lipid homeostasis and being correlated to the cancer cell growth and progression. Cholesterol (CH) is stored in lipid droplets and the expression of genes related to the CH regulation can be modified. Studies have shown that high levels of lipids can affect the cancer development. It has been also demonstrated that oleic acid (OA) has an inhibitory effect on cancer cells. The present study aimed to investigate the effects of exogenous supplementation of CH, OA and a combination of CH + OA on the invasive behavior of canine osteosarcoma cells (OSCA40) *in vitro*. Therefore, we performed two-dimensional (2D) and three-dimensional (3D) invasion assays, western blot (WB) and immunohistochemical detection of PLIN1, PLIN2, PLIN3 and PLIN5 and qRT-PCR in microtumor models (spheroids) of the OSCA40 cells *in vitro* within the respective treatment groups.

An increase of cell invasion was observed upon CH and CH + OA treatment compared to the control group (C) within the 2D invasion assays. Comparable effects were observed in a time dependent manner within the 3D invasion assays experiments. A decrease in gene expression level of adenosine triphosphate binding cassette transporter A1 (ABCA1) and sterol regulatory element binding protein 1 (SREBF1) was detected through qRT-PCR. In immunohistochemical analyses, a decrease of Ki67 protein indicating a reduction of proliferative activity in OSCA40 spheroids stimulated with CH + OA in relation to C was detected. The WB analyses did not detect any variations of PLIN2 and PLIN3 in the treated cells. A high inter-experimental variability of the observed effects has to be mentioned for all of the applied techniques.

Our results indicate that the exogenous lipids actually may feature pro-tumorigenic effects in canine OSCA40 osteosarcoma cells *in vitro*, but more tests are necessary to rule out possible technical interferences and to determine significant effects of the lipogenic stimulation.

7 Zusammenfassung

Osteosarkome sind die häufigste Art von Knochenkrebs, hochaggressiv und breiten sich bei metastasierenden Erkrankungen häufig auf Lungen und andere Knochen aus. Veränderungen im Lipidstoffwechsel können mit Krebs zusammenhängen, da Lipide für Krebszellen als Energiespeicher und Signalweg notwendig sind. Lipidtröpfchen sind an der Ansammlung und dem Stoffwechsel von Lipiden beteiligt. Lipidtröpfchen werden von Hüllproteinen, wie zum Beispiel den Perilipinen (PLINs) umgeben. Diese steuern die zelluläre Lipidhomöostase und korrelieren mit dem Wachstum und der Progression von verschiedenen Typen von Krebszellen. Cholesterin (CH) wird in Lipidtröpfchen gespeichert und die Expression von Genen, die mit der CH-Regulation zusammenhängen, kann durch maligne Transformation der Zellen modifiziert werden. Studien haben gezeigt, dass hohe intrazelluläre Lipidspiegel die Krebsentstehung beeinflussen können. Es wurde jedoch auch gezeigt, dass Ölsäure (OA) eine hemmende Wirkung auf unterschiedliche Krebszellen hat. Das Ziel der vorliegenden Studie war die Untersuchung der potentiellen Auswirkungen einer exogenen Stimulation durch CH, OA und einer Kombination von CH + OA auf das invasive Verhalten von caninen Osteosarkom Zellen (OSCA40 Zelllinie) *in vitro* zu untersuchen. Daher führten wir zweidimensionale (2D) und dreidimensionale (3D) Invasionsassays, Western Blot (WB) Analysen und immunhistochemische Nachweise von PLIN1, PLIN2, PLIN3 und PLIN5 sowie qRT-PCR in Mikrotumor-Modellen (Sphäroide) der OSCA40-Zellen *in vitro* innerhalb der jeweiligen Behandlungsgruppen durch.

Eine Zunahme der Zellinvasion wurde bei CH- und CH+OA-Behandlung im Vergleich zur Kontrollgruppe (C) innerhalb der 2D-Invasionsassays beobachtet. Vergleichbare Effekte wurden zeitabhängig in den Experimenten mit 3D-Invasionsassays beobachtet. Eine Abnahme des Genexpressionsniveaus von Adenosintriphosphat-Bindungskassettentransporter A1 (ABCA1) und Sterolregulationselement-Bindungsprotein 1 (SREBF1) wurde durch qRT-PCR nachgewiesen. In immunhistochemischen Analysen wurde eine Abnahme des Ki67-Proteins in mit CH + OA stimulierten OSCA40-Sphäroiden in Bezug auf C festgestellt, welche eine Reduktion der proliferativen Aktivität in diesen Gruppen darstellt. Die WB-Analysen ergaben keine Variation von PLIN2 und PLIN3 in den behandelten Zellen. Eine hohe interexperimentelle Variabilität der beobachteten Effekte muss erwähnt werden.

Unsere Ergebnisse zeigten, dass die exogenen Lipide *in vitro* scheinbar pro-tumorigene Wirkungen in OSCA40-Osteosarkomzellen von Hunden aufweisen können. Es sind jedoch weitere Tests erforderlich, um mögliche technische Interferenzen auszuschließen und signifikante Wirkungen der lipogenen Stimulation zu bestimmen.

8 List of Abbreviations

% t0	Invasion activity
◦C	Degree Celsius
µl	Microliter
2D	Two-dimensional
3D	Three-dimensional
ABCA1	ATP-binding cassette transporter A1
AGPAT9	1-acylglycerol-3-phosphate O-acyltransferase
AMP	Adenosine monophosphate
bHLH	Basic helix-loop-helix
C	Control
C+	Positive control
C-	Negative control
cDNA	Complementary DNA
CH	Cholesterol
CO_2	Carbon dioxide
Ct	Cycle threshold
DAB	Diaminobenzidine
DMEM	Dulbecco's Modified Eagle Medium
EMT	Epithelial to mesenchymal transition
ECL	Enhanced Chemiluminescence
ERK	Extracellular signal-regulated kinase
et al.	et alii
Exp 1	Experiment 1
Exp 2	Experiment 2
Exp 3	Experiment 3
FCS	Fetal calf serum
FFPE	Formalin fixed and paraffin embedded
Fig.	Figure
g	Frequency
GPAT3	Glycerol-3-phosphate acyltransferase 3
GSK3B	Glycogen synthase kinase 3 beta
H & E	Hematoxylin and Eosin
H_2O_2	Hydrogen peroxide
HeLa	Human cervical cancer cell line
HF MM	High-Fidelity mastermix
IHC	Immunohistochemistry
IPP	Isopentenyl pyrophosphate
LDL	Low density lipid
M	Molarity
MEK	Mitogen-activated protein kinase

MGLL	Monoglyceride lipase
ml	Milliliter
MYC	Proto-oncogene, bHLH transcription facto
NaCl	Sodium chloride
NF-κB	Nuclear factor kappa B
OA	Oleic acid
OAZ1	Ornithine decarboxylase antizyme 1
OLR1	Oxidized low-density lipoprotein receptor 1
OSCA40	Canine osteosarcoma cell line
PBS	Phosphate-buffered saline
pH	Power of hydrogen
PLIN	Perilipin
PPAP2C	Phospholipid phosphatase 2
PVDF	Polyvinylidene difluoride
qRT-PCR	Quantitative reverse transcription polymerase chain reaction
RIPA	Radioimmunoprecipitation assay
RPL27	Ribosomal Protein L27
RT	Reverse transcriptase
Saos-2	Human osteosarcoma cell line
SCARB2	Scavenger receptor class B member 2
SDS	Sodium dodecyl sulfate
SDS-PAGE	Sulfate polyacrylamide gel electrophoresis
SREBP-1	Sterol regulatory element binding protein 1
T75	Tissue culture flasks 75
Tab.	Table
TBST	Tris-Buffered-Saline-Tween
Tris HCL	Tris hydrochloride
USF2	Upstream transcription factor 2, c-fos interacting
vs.	Versus
WB	Western blot
ΔCt	Delta Ct

9 List of Tables

10 List of Figures